

**This item is the archived peer-reviewed author-version of:**

Elevated sedimentary removal of Fe, Mn, and trace elements following a transient oxygenation event in the Eastern Gotland Basin, central Baltic Sea

**Reference:**

van de Velde Sebastiaan J., Huyen Astrid, Kononets Mikhail, Marzocchi Ugo, Leermakers Martine, Choumiline Konstantin, Hall Per O. J., Meysman Filip.- Elevated sedimentary removal of Fe, Mn, and trace elements following a transient oxygenation event in the Eastern Gotland Basin, central Baltic Sea  
Geochimica et cosmochimica acta - ISSN 0016-7037 - 271(2020), p. 16-32  
Full text (Publisher's DOI): <https://doi.org/10.1016/J.GCA.2019.11.034>  
To cite this reference: <https://hdl.handle.net/10067/1656470151162165141>

## Journal Pre-proofs

Elevated sedimentary removal of Fe, Mn, and trace elements following a transient oxygenation event in the Eastern Gotland Basin, central Baltic Sea

Sebastiaan van de Velde, Astrid Hylén, Mikhail Kononets, Ugo Marzocchi, Martine Leermakers, Konstantin Choumiline, Per O.J. Hall, Filip J.R. Meysman

PII: S0016-7037(19)30742-2  
DOI: <https://doi.org/10.1016/j.gca.2019.11.034>  
Reference: GCA 11546

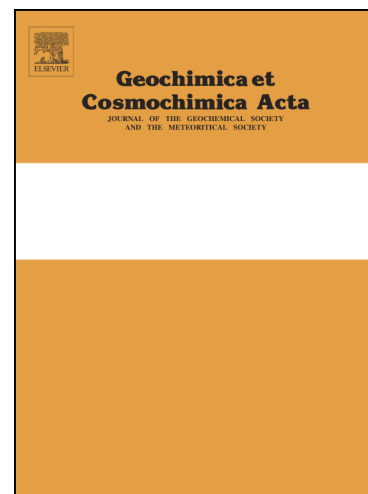
To appear in: *Geochimica et Cosmochimica Acta*

Received Date: 14 February 2019  
Revised Date: 26 November 2019  
Accepted Date: 27 November 2019

Please cite this article as: van de Velde, S., Hylén, A., Kononets, M., Marzocchi, U., Leermakers, M., Choumiline, K., Hall, P.O.J., Meysman, F.J.R., Elevated sedimentary removal of Fe, Mn, and trace elements following a transient oxygenation event in the Eastern Gotland Basin, central Baltic Sea, *Geochimica et Cosmochimica Acta* (2019), doi: <https://doi.org/10.1016/j.gca.2019.11.034>

This is a PDF file of an article that has undergone enhancements after acceptance, such as the addition of a cover page and metadata, and formatting for readability, but it is not yet the definitive version of record. This version will undergo additional copyediting, typesetting and review before it is published in its final form, but we are providing this version to give early visibility of the article. Please note that, during the production process, errors may be discovered which could affect the content, and all legal disclaimers that apply to the journal pertain.

© 2019 Elsevier Ltd. All rights reserved.



# Elevated sedimentary removal of Fe, Mn, and trace elements following a transient oxygenation event in the Eastern Gotland Basin, central Baltic Sea

Sebastiaan van de Velde <sup>1,2#</sup>

Astrid Hylén <sup>3</sup>

Mikhail Kononets <sup>3</sup>

Ugo Marzocchi <sup>2,4</sup>

Martine Leermakers <sup>2</sup>

Konstantin Choumiline <sup>1</sup>

Per O. J. Hall <sup>3</sup>

Filip J. R. Meysman<sup>5,6</sup>

<sup>1</sup> Department of Earth and Planetary Sciences, University of California, Riverside, CA 92521, USA

<sup>2</sup> Department of Chemistry, Vrije Universiteit Brussel, 1050 Brussel, Belgium

<sup>3</sup> Department of Marine Sciences, University of Gothenburg, Box 461, 413 19 Gothenburg, Sweden

<sup>4</sup> Center for Electromicrobiology, Department of Bioscience, Aarhus University, 8000 Aarhus, Denmark

<sup>5</sup> Department of Biology, University of Antwerp, 2160 Wilrijk, Belgium

<sup>6</sup> Department of Biotechnology, Delft University of Technology, Delft, The Netherlands

# Corresponding author: sebastiv@ucr.edu (Tel. +1 951 394 5205)

**Submitted to:** *Geochimica Cosmochimica Acta*

**Keywords:** Baltic Sea, Eastern Gotland Basin, Major Baltic Inflows, GEOTRACES

**Version:** revised version 02 (26/11/2019)

**Word count:** Abstract: 371 / Text: 8601

**ABSTRACT**

Iron, manganese, and trace elements play an important role in the marine carbon cycle as they are limiting nutrients for marine primary productivity. Water column concentrations of these bio-essential elements are controlled by the balance between input and removal, with burial in marine sediments being the main sink. The efficiency of this burial sink is dependent on the redox state of the water column, with sediments underlying a sulphidic (euxinic) water column being the most efficient sinks for Fe, but also Mn and trace elements (Co, Cd, Ni, Mo, As, W, V, and U). Transient changes in ocean redox state can hence affect trace element burial, and correspondingly, the ocean's trace element inventory, but the impact of transient oxygenation events on trace element cycling is currently not well understood.

Here, we investigate the impact of a natural oxygenation event on trace element release and burial in sediments of the Eastern Gotland Basin (EGB), a sub-basin of the Baltic Sea. After being anoxic ( $< 0.5 \mu\text{M O}_2$ ) for  $\sim 10$  years, the deep waters of the EGB experienced a natural oxygenation event (Major Baltic Inflow, MBI) in 2015. Following this oxygenation event, we deployed benthic chamber landers along a depth transect in the EGB in April 2016, 2017 and 2018. We complemented these *in situ* flux measurements with analyses of water column, solid phase and pore water chemistry. Overall, the event increased the benthic effluxes of dissolved trace elements, though particular responses were element-specific and were caused by different mechanisms. Enhanced fluxes of Cd and U were caused by oxidative remobilisation, while Ni showed little response to the inflow of oxygen. In contrast, enhanced release of Co, Mo, As, W, and V was caused by the enhanced transient input of Mn oxides into the sediment, whereas Fe oxides were of minor importance. Following the dissolution of the oxides in the sediment, Mn and W were nearly completely recycled back to the water column, while fractions of Fe, Co, Mo, As, and V were retained in the sediment. Our results suggest that transient oxygenation events in euxinic basins may decrease the water column inventory of certain trace elements (Fe, Co, Mo, As, and V), thus potentially affecting global marine primary productivity on longer timescales.

## 1. INTRODUCTION

The biogeochemical cycling of iron (Fe), manganese (Mn), and trace elements plays a vital role in marine ecosystems and the global carbon cycle (GEOTRACES, 2006). Most trace elements are essential nutrients and despite their abundance in the Earth's crust, they are limiting nutrients for primary production (McLennan, 2001; Morel and Price, 2003; Mahowald et al., 2018; Baeyens et al., 2018). This apparent paradox is caused by the restricted supply of dissolved trace elements to the ocean. Aerosol deposition has typically been considered the dominant source for trace elements into the open ocean (Jickells, 2005), though other mechanisms are also increasingly considered. Fluvial and hydrothermal pathways can be significant in certain regions of the ocean (Buck et al., 2007; Jones et al., 2011; Fitzsimmons et al., 2017), while shelf-to-basin shuttling is thought to be an important source of Fe for pelagic primary production in the open ocean (Elrod et al., 2004; Severmann et al., 2010; Dale et al., 2015; Klar et al., 2017). In the ocean, these sources are counterbalanced by burial in sediments, which represents a permanent sink for Fe, Mn and trace elements. The efficiency of sediment burial controls the water column concentrations and depends largely on the redox state of the overlying water column.

Under oxic conditions, Fe and Mn form insoluble oxides (Thamdrup, 2000), while they exist as dissolved  $Mn^{2+}$  and  $Fe^{2+}$  or form reduced minerals under anoxic ( $< 0.5 \mu M O_2$ ) conditions. Sediments deposited under an oxygenated water column generally lose a fraction of their particulate Fe and Mn (oxyhydr)oxides as a dissolved benthic flux to the overlying water column (Elrod et al., 2004; Lyons and Severmann, 2006). These benthic effluxes are stimulated by bioturbation, in particular by the activity of bio-irrigating macrofauna that flush their burrow systems (van de Velde and Meysman, 2016; Thibault de Chanvalon et al., 2017; Lenstra et al., 2018). In contrast, sediments underlying anoxic waters with free hydrogen sulphide (euxinia) act as permanent sinks for Fe through precipitation of FeS minerals in the water column and subsequent burial in the sediment (Anderson and Raiswell, 2004; Lyons and Severmann, 2006). This redox behaviour is important for local Fe transport, so called 'shelf-to-basin shuttling'. Iron that is reduced in deeper, anoxic parts of coastal shelf sediments and is released to an oxic water column can be transported further offshore in dissolved form, before it is oxidised and forms particulate Fe. The Fe oxides can aggregate and sink to the sediment again, and by this mechanism Fe may undergo several oxidation-reduction cycles as it is "shuttled" further offshore. Manganese also exhibits a similar shuttling behaviour (Lyons and Severmann, 2006;

Jilbert and Slomp, 2013; Scholz et al., 2013; Dijkstra et al., 2016), while physical transport via deposition-resuspension cycles is important for shelf sediments with a relatively low organic matter input (Lenstra et al., 2018).

Trace elements can respond directly or indirectly to redox changes and their behaviour depends primarily on their physico-chemical properties. **Cobalt (Co), Cadmium (Cd) and Nickel (Ni)** belong to the category of divalent cations that are unlikely to undergo redox reactions but are particle-reactive. All three elements form complexes with organic ligands or dissolved anions and can be scavenged by particles (organic matter, Fe and Mn oxides). In the presence of dissolved sulphide, they can form insoluble sulphide minerals and become incorporated in pyrite (Huerta-diaz and Morse, 1992; Morford and Emerson, 1999; Saito and Moffett, 2001; Piper and Perkins, 2004; Tribovillard et al., 2006). Note that  $\text{Co}^{2+}$  has been shown to oxidise to  $\text{Co}^{3+}$  in the presence of Mn oxides (Lee and Tebo, 1994; Moffett and Ho, 1996; Murray et al., 2007), but the presence of organic or inorganic ligands in natural water stabilises the reduced  $\text{Co}^{2+}$  form (Saito and Moffett, 2001). **Molybdenum (Mo), Arsenic (As) and Tungsten (W)** are a group of metalloids that form oxyanions under oxic conditions, and which efficiently adsorb onto Fe and Mn oxides (Bertine, 1972; Gustafsson, 2003; Giménez et al., 2007). The oxygen atoms in the oxyanion complex can be replaced by dissolved sulphide, which leads to the formation of thio-complexes and concomitant changes in adsorption properties. While thio-molybdate is highly particle-reactive (Tribovillard et al., 2004; Vorlicek et al., 2004; Tribovillard et al., 2006), the thio-complexes of both As and W are less prone to particle scavenging (Kirk et al., 2010; Cui and Johannesson, 2017), although As does co-precipitate with pyrite (Huerta-diaz and Morse, 1992). **Vanadium (V) and Uranium (U)** belong to a category of trace elements that are somewhat particle reactive in their oxidised forms and can adsorb onto Fe and Mn oxides (Wehrli and Stumm, 1989a; Waite et al., 1994; Hastings et al., 1996; Wang et al., 2013). In their reduced form, these elements precipitate as solid oxide or hydroxide phases (Klinkhammer and Palmer, 1991; Wanty and Goldhaber, 1992; Morford and Emerson, 1999; Cumberland et al., 2016).

Changes in the oxygenation state of the water column will likely affect the availability of Fe, Mn and trace elements in the ocean. In the coming decades, oceanic oxygen concentrations are expected to decrease, whereas anoxic and euxinic zones are expected to increase in size (Keeling et al., 2010). The extent of an oxygen minimum zone (OMZ) is not fixed in time and space (Scholz et al., 2011), and the anoxic or euxinic conditions within the most pronounced of

these OMZs (e.g. offshore Mexico and Peru; Scholz et al., 2014) will thus experience transient reoxygenation events. This will affect the sink/source behaviour of marine sediments, and consequently the trace element inventory in the ocean (Scholz et al., 2014). However, detailed studies of the impact of transient bottom-water reoxygenation of euxinic bottom waters on the sedimentary release of trace elements are rare. The available studies remain generally restricted to Fe, Mn (Hermans et al., 2019) and paleo-proxies (V, Mo and U; Scholz et al., 2011; Scholz et al., 2018), with no *in situ* quantification of trace element release using benthic landers.

Here, our aim was to investigate the impact of a natural transient reoxygenation event in the long-term euxinic Eastern Gotland Basin (EGB), a sub-basin of the central Baltic Sea, on the sedimentary release and retention of Fe, Mn and trace elements (As, Cd, Co, Mo, Ni, U, V, W). These elements have importance for biology or as paleo-proxies, represent different physico-chemical groups, and sedimentary effluxes can be measured with sufficient accuracy using the methods we employed. We followed the evolution of Fe, Mn and trace element diagenesis after the transient re-oxygenation during campaigns in three consecutive years, using a combination of *in situ* measured benthic fluxes, water column, and pore water sampling and solid phase analysis.

## 2. MATERIALS & METHODS

### 2.1 Field site

The EGB is situated in the central part of the Baltic Sea, between Latvia and the island of Gotland (Sweden) (Fig. 1). It is the largest sub-basin of the Baltic Proper (the central part of the Baltic Sea), with a maximum water depth of 249 m and a strong and permanent halocline at approximately 60-80 m depth. The EGB is heavily affected by eutrophication, which in combination with a strong stratification of the water column has led to prolonged periods of anoxia ( $[O_2] < 0.5 \mu\text{M}$ ) below the halocline. The sediments above the halocline (< 80 m depth) are strongly affected by waves and bottom currents and are generally classified as erosion-transport bottoms. These shallow sediments show no net long-term sediment accumulation and consist of coarser sand since finer material is rapidly eroded and transported to the deeper basin (Carman and Cederwall, 2001; Nilsson et al., 2018). Below the halocline (> 80 m depth), fine sediment accumulates at a rate of  $\sim 0.1 \text{ cm yr}^{-1}$  (Hille et al., 2006).



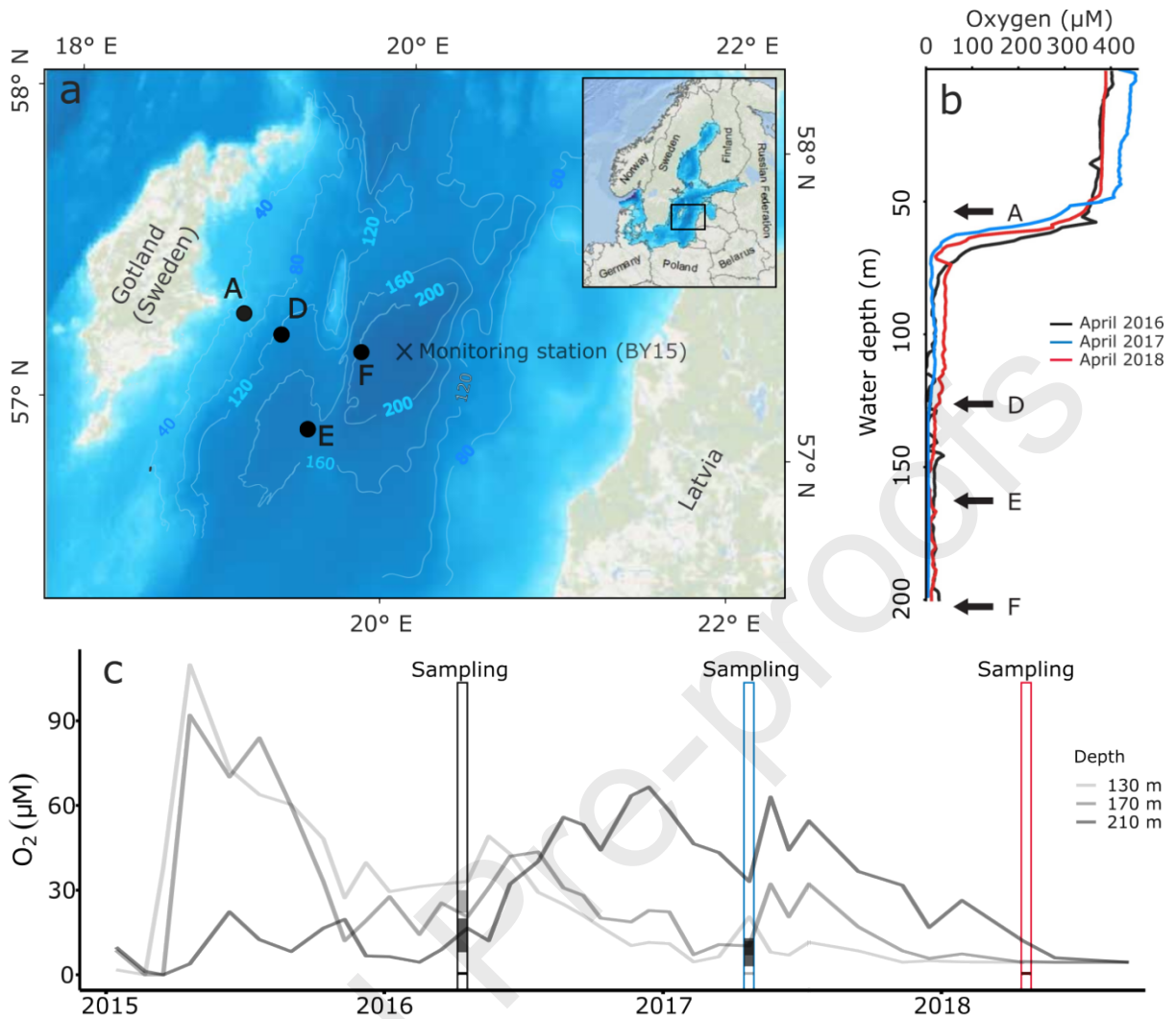


**Figure 1:** (a) Map of the Eastern Gotland Basin with the locations of the sampling stations (A, D, E and F), as well as the position of the monitoring station where the oxygen time series of panel c was recorded (BY15). (b) Oxygen depth profiles recorded in April 2016, 2017 and 2018. Arrows indicate water depth of the stations. Bathymetry was taken from the Baltic Sea Bathymetry Database (BSBD; <http://data.bsbc.pro>). (c) Variability of oxygen concentrations through time at the following water depths: 130 m, 170 m, and 210 m obtained from the Swedish Meteorological and Hydrological Institute website (<https://sharkweb.smhi.se/>) at station BY15. These water depths correspond to the bottom depth of our sediment sampling sites. Coloured bars indicate sampling periods; greyscale on bars indicate oxygen concentrations recorded by our benthic landers at each station. During the 2018 sampling, all measured oxygen concentrations were below LOD ( $<0.5 \mu\text{M}$ ).

In 2014, a large inflow of dense and oxygenated water from the North Sea, a so called major Baltic inflow (MBI), entered the Baltic Sea (Mohrholz et al., 2015). This MBI reached the EGB in March 2015 and temporarily re-oxygenated the waters below 140 m depth, after 10 years of preceding anoxia (Fig. 1c ; Hall et al., 2017; Liblik et al., 2018). The newly brought oxygen was consumed by October 2015, but the bottom water oxygen levels increased again in March



2016, when a smaller inflow reached the EGB. However, by March 2017, the oxygen had mostly disappeared again (Fig. 1c; Liblik et al., 2018). Over the period 2015-2018, several smaller inflows were recorded at ~120 m depth in the EGB (Fig. 1c; Liblik et al., 2018).

## 2.2 Benthic lander deployments and *in situ* water measurements

The EGB was visited during separate sampling campaigns aboard the R/V Skagerak in three consecutive years (April 2016, 2017 and 2018; Fig 1c). Benthic chamber landers were deployed at stations A (60 m water depth), D (130 m water depth), E (170 m water depth) and F (210 m water depth) (Fig. 1a,b). Landers were deployed twice per location during each campaign, with a few exceptions due to ship time scheduling or weather constraints (Table 1). Before each lander deployment, water column depth profiles of temperature, salinity and oxygen were recorded using a CTD instrument (SBE 911, Sea-Bird Scientific) equipped with a high-accuracy oxygen sensor (SBE 43, Sea-Bird Scientific).

Water column samples were collected using 5 L NISKIN bottles attached to a CTD carousel during one deployment in 2017 at the deepest station (F; 210 m water depth). Water samples were collected at discrete depths (5 m, 15 m, 30 m, 40 m, 60 m, 80 m, 100 m, 120 m, 140 m, 160 m, 180 m and 200 m). One litre of bottom water per sampled depth was filtered through pre-weighed polyethersulphone (PES) filters (0.45  $\mu\text{m}$  pore size, Supor, PALL) by pressure filtration using 50 mL syringes (PP). Filtrate was collected in two different 500 mL acid-cleaned LDPE bottles (Nalgene™) per sample depth.

Solute fluxes across the sediment-water interface were measured by collecting water samples *in situ* using the autonomous Gothenburg benthic lander (Tengberg et al., 2004; Almroth et al., 2009; Kononets et al., *subm.*). This lander carried four benthic chambers, each incubating a sediment surface area of  $A_{\text{chamber}} = 400 \text{ cm}^2$ . The overlying water was stirred with a horizontal paddle wheel to prevent the build-up of concentration gradients in the chamber. Nine syringes (PP) allowed sampling of the overlying water in each chamber at pre-set times. The syringes were cleaned with milli-Q before deployment, as previous tests indicated that acid-washing syringes led to random contamination effects. Blank incubations (lander incubations without sediment) using syringes that were rinsed using milli-Q water showed that trace elements did not leach from the materials used in the lander (Supplementary Fig. 1, Appendix 2). Ambient bottom water entered the chamber through a small stainless-steel loop as samples were withdrawn. Sensors mounted inside and outside of the chambers monitored the oxygen

concentration (Oxygen Optode 3830; Aanderaa Data Instruments), turbidity (Turbidity Sensor Model 3612A; Aanderaa Data Instruments), conductivity, and temperature (Sensor 3919; Aanderaa Data Instruments). The volume ( $V_{\text{chamber}}$ ) of overlying water in each chamber was calculated from the decrease in salinity following the injection of a known volume of milli-Q water ( $V_{\text{injection}}$ ) corresponding to 0.5-1 % of the total chamber volume (Kononets et al., *subm.*):

$$V_{\text{chamber}} = V_{\text{injection}} \frac{S_{\text{before}}}{S_{\text{before}} - S_{\text{after}}} \quad [1]$$

where  $S_{\text{before}}$  and  $S_{\text{after}}$  are the salinities before and after the injection, respectively. The chamber water height (necessary to calculate the benthic flux) was calculated as  $H = V_{\text{chamber}}/A_{\text{chamber}}$ , where  $A$  is the incubated surface area (relative uncertainty: 6-12%). This procedure has been tested at a salinity of  $\sim 2.5$ , at which the freshening of chamber water is still measurable (Kononets et al., *subm.*).

Before the start of each incubation, the lander frame was left hanging for 2 hours at a depth of  $\sim 1$  m above the seafloor with open chambers that were actively stirred. During that time, a 5 L NISKIN flask attached to the frame was used to sample bottom water before the deployment of the lander. After this 2h waiting period, the lander frame was slowly lowered to the seafloor and the chambers were inserted into the sediment with the chamber lid open and continuous stirring for another 2 hours. These pre-incubation steps ensured that ambient bottom water was incubated and that any oxygen contained in the polycarbonate chamber walls equilibrated with the surrounding environment. After the chamber lid was closed, sediment and water were incubated for 37 hours at station A and 14 hours at stations D, E and F. Immediately after lander recovery, syringe samples were filtered in open air through pre-rinsed cellulose acetate filters (Sartorius, 0.45  $\mu\text{m}$  pore size). Bottom water collected by the NISKIN flask was processed as described before for the water column samples.

Benthic fluxes of dissolved trace elements were calculated from their concentration change in the chamber water over time. Concentrations were corrected for the small dilution that took place when new bottom water entered the chamber during syringe sampling. A linear or quadratic least-square regression line was fitted to concentration data versus time (selected based on highest adjusted  $R^2$  value, which was adjusted for the number of predictors in the model; see below). When a quadratic fit was selected, the flux was calculated only for the first time point, which gives the flux at the start of the deployment. Data points with high leverage were identified through the calculation of Studentized Deleted Residual Index (SDRI) and

Cook's distance values (Belsley et al. 1980; Cook and Weisberg 1982; Williams 1987). Points with a SDRI higher than 2 and Cook's distance higher than  $4/(n-2)$ , where  $n$  is the number of data points were considered outliers and were removed. Diagnostic graphs of residuals were used to verify that the assumptions of the regression were fulfilled (e.g. random distribution of residuals, distribution of residuals has a constant variance). All analysis was done in the open source software R using the 'lm' and 'nls' functions from the built-in CRAN:stats package (R Core Team, 2017). The flux across the sediment-water interface was calculated by multiplying the chamber water height with the initial slope of the regression line. Fluxes with  $p$ -values  $< 0.05$  were considered to differ significantly from a zero flux. For a detailed discussion of the flux evaluation method, see Hylén et al. (subm.).

### 2.3 Sediment sampling

Sediment was retrieved during each sampling campaign at all stations using a modified box corer (Blomqvist et al., 2015). Six subcores were manually collected from several box cores using transparent PVC core liners (inner diameter 60 mm; length 30 cm). Sediment cores were closed with a rubber stopper from the bottom and were temporarily stored with an open top in an incubation tank filled with bottom water collected from the sampling site. The tank was equipped with a temperature controller that kept the water at *in situ* temperature. Oxygen concentrations were continuously monitored by an optic sensor (Oxygen Optode 3830; Aanderaa Data Instruments). To keep the *in situ*  $O_2$  concentration, the water was bubbled with a  $N_2/CO_2$  mixture at an intensity that was manually adjusted to keep the correct  $O_2$  concentration.

After a ~6 hours transit back to the harbour, sample processing started onboard. Two cores from each station were sectioned immediately for pore water extraction under  $N_2$  atmosphere in a portable glove bag (Captair Pyramid, Erlab, France). Oxygen concentrations in the glove bag were continuously monitored (Portable Oxygen Analyzer Model 3110; Teledyne Analytical Instruments). Sediment slicing was performed at 0.5 cm resolution from 0 to 3 cm depth, at 1 cm resolution between 3 and 10 cm depth, and in 2 cm slices from 10 to 14 cm depth. Sediment sections were collected in 50 mL centrifuge tubes (polypropylene; Techno Plastic Products, Switzerland) and pore water was extracted by two different methods depending on the campaign. In the first campaign (April 2016), the 50 mL tubes were centrifuged at 2500 g for 10 min (Sigma 3-16L, Sigma Laborzentrifugen GmbH, Germany). Subsequently, the

centrifuge tubes were opened in the anoxic glove bag and overlying pore water was transferred into suitable sample containers after filtration through 0.45  $\mu\text{m}$  pore size cellulose acetate filters (CHROMAFIL Xtra; MACHERY-NAGEL, Germany). During the subsequent campaigns (April 2017 and April 2018), pore water was extracted from the centrifuge tubes by Rhizon samplers (pore size  $\sim 0.15 \mu\text{m}$ ; Rhizosphere Research Products, The Netherlands), which allowed us to extract more pore water than the centrifugation method. In the glove bag, Rhizons were manually inserted into the tubes until the porous part was completely covered by sediment. Syringes attached to the Rhizons were drawn back and fixed in this position, creating a vacuum which extracted the pore water. Afterwards, sample volume was distributed into sample containers without filtration.

## 2.4 Sediment physical parameters

Individual sediment cores were collected with a custom-made multi-corer for the determination of porosity depth profiles at all stations in each sampling campaign. The cores (inner diameter 9.9 cm) were sliced at 0.5 cm resolution between 0 and 2 cm depth, at 1 cm resolution between 2 and 6 cm depth and 2 cm between 6 and 10 cm depth. The water content of each sediment section was obtained from the weight loss after drying the samples at 70  $^{\circ}\text{C}$  until constant weight (at least 48 h). The solid-phase density was determined by recording the mass difference between a 25 mL volumetric flask filled with only milli-Q water ( $m_{MQ}$ ) and the same flask with a known mass of homogenised freeze-dried sediment ( $m_{sed}$ ) and filled with milli-Q water to the same volume ( $m_{MQ+sed}$ ). The volume of the added sediment was then calculated as

$$V_{sed} = \frac{[m_{MQ} - (m_{MQ+sed} - m_{sed})]}{\rho_{H_2O}} \quad [1]$$

where  $\rho_{H_2O}$  is the density of water. The sediment density was subsequently calculated as  $\rho_{sed} = m_{sed} / V_{sed}$ . Sediment porosity (volume of pore water per volume of bulk sediment) was determined from water content and solid-phase density, accounting for the salt content of the pore water.

## 2.5 Water column, chamber water and pore water analysis

Water samples for determination of dissolved elemental composition (As, Co, Cd, Fe, Mn, Mo, Ni, U, V, W) were stabilised with 50  $\mu\text{L}/\text{mL}$  bidistilled  $\text{HNO}_3$  (65%, Suprapure, Merck; final  $\text{HNO}_3$  concentration was  $\sim 3\%$ ) and stored at  $4^\circ\text{C}$ . In 2016, the acid to sample ratio for the pore water samples was 100  $\mu\text{L}/\text{mL}$ , which we decreased to 50  $\mu\text{L}/\text{mL}$  in the subsequent years. In 2016, the samples were diluted 20 times with a 1% aqueous  $\text{HNO}_3$  solution prior to analysis. In the subsequent years, the dilution factor was reduced to 10 times, which increased the performance of our method (Supplementary Table 3, Appendix 1). The analysis was done by High Resolution Inductively Coupled Plasma Mass Spectrometry (HR-ICP-MS; Element 2, ThermoFisher Scientific). Indium (2.5 ppb) containing 2%  $\text{HNO}_3$  was injected simultaneously with the samples as an internal standard (the detection and quantification limits for each metal are shown in Supplementary Table 1, Appendix 1). Before each run, certified reference material (SLEW-3, estuarine water, National Research Council Canada; SLRS-6, river water, National Research Council Canada; NIST 1640a, natural water, National Institute for Standards and Technology, USA) was diluted in the same fashion as the samples and analysed to monitor the precision and accuracy of the method (Supplementary Table 3; Appendix 1). It should be noted that HR-ICP-MS analysis provides total elemental concentrations. In this paper, we use the operational term ‘dissolved’, referring to the fraction that either passed through a 0.45  $\mu\text{m}$  filter (2016 campaign) or a Rhizon sampler with pore size  $\sim 0.15 \mu\text{m}$  (2017/2018 campaigns).

## 2.6 Solid-phase and filter analysis

In the 2016 campaign, the solid phase that remained after centrifugation was freeze-dried and stored in aluminium bags under  $\text{N}_2$  atmosphere for later analysis. Only 2016 samples were used, as we did not expect to see any change in total trace element contents between samplings. Total contents of (trace) elements (Al, As, Cd, Co, Fe, Mn, Mo, Ni, Ti, U, V, and W) were determined by total digestion. Freeze-dried subsamples (300 mg) were homogenised and dissolved by microwave-assisted digestion (CEM Mars 5) using 12 mL of an acid mixture ( $\text{HF}/\text{HCl}/\text{HNO}_3$  in a 2:1:3 ratio), followed by a second neutralising step using 30 mL  $\text{H}_3\text{BO}_3$  (US EPA method 3052). Certified Reference Material (MESS-3: Marine Sediment, National Research Council Canada) and method blanks were included in every digestion run to monitor precision and accuracy of the extractions (Supplementary Tables 2 and 3; Appendix 1). Subsequently, total digests were analysed for Al, Ti and Fe by Inductively Coupled Plasma

Optical Emission Spectrometry (Iris Advantage ICP-OES, Thermo Scientific) after 100-fold dilution and using 0.2 ppm gold and ytterbium as internal standards. The precision of the method was < 10% (all precisions are calculated as one relative standard deviation), accuracy for each element is reported in Supplementary Table 3 (Appendix 1). For trace elements (As, Cd, Co, Mn, Mo, Ni, U, V, W) the total digests were analysed by HR-ICP-MS as described in section 2.5. In 2017, the material remaining on the filter after filtration of water column samples was oven-dried to constant weight (70°C) and digested following an identical method as described for the solid phase samples.

Freeze-dried samples from the 2016 campaign were also analysed for particulate organic carbon (POC) by a Thermo1112 Flash elemental analyser. Samples were acidified before each analysis with 0.1N HCl to remove the inorganic carbon (Nieuwenhuize et al., 1994). The POC values are expressed as mass % of dry weight of the sediment sample. The precision was < 5% for the POC measurements.

**Table 1:** Summary of bottom water data. Salinity (S), temperature (T, °C) and oxygen (O<sub>2</sub>, μM) as measured by sensors on the benthic chamber lander less than 0.5 m above seafloor. The range of recorded values is given over the deployment period. Limit of Detection (LOD) for oxygen = 0.5 μM. D1= first deployment, D2 = second deployment; missing values indicate that only one deployment was done that year. Values in italics are CTD values replacing lander values, due to issues with conductivity/salinity sensor on the lander during deployment.

Station	Coordinates	Depth	Year	Salinity		Temperature (°C)		O <sub>2</sub> concentration (μM)	
				D1	D2	D1	D2	D1	D2
A	N 57°23.11' E 19°04.95'	60m	2016	7.25-7.35	-	3.60-3.90	-	330-350	-
			2017	7.7	8.9	4.00-5.00	5.0	100-120	300
	2018	7.42-7.50	7.5	2.70-3.00	2.60-3.00	330-355	325-350		
D	N 57°19.67' E 19°19.41'	130m	2016	12.5-12.70	12.55-12.65	6.50-6.60	6.50-6.60	<0.5	<0.5
			2017	12.7	12.7	6.72-6.76	6.7	8-13	9
			2018	12.50-12.55	12.40-12.50	6.65-6.85	6.60-6.80	<0.5	<0.5
E	N 57°01.52' E 19°30.45'	170m	2016	12.96-12.99	12.90-13.10	6.75-6.85	6.75-6.85	8-20	7-10
			2017	13.1	13.1	6.91-6.95	7.00-7.20	6-13	3-8
			2018	13.05-13.15	-	6.80-7.10	-	<0.5	-
F	N 57°17.22' E 19°48.04'	210m	2016	13.82-13.86	13.75-13.85	7.38-7.43	7.34-7.38	22-30	23-27
			2017	13.5	-	7.20-7.40	-	<0.5	-
			2018	13.12-13.18	13.24-13.29	6.90-7.05	6.90-7.05	<0.5	<0.5

### 3. RESULTS

#### 3.1 Bottom water conditions

We visited four stations in the EGB (Fig. 1a) during three annual sampling campaigns in April 2016, 2017, and 2018 (Table 1). Station A was situated just above the halocline and had oxygenated bottom waters on all occasions. In 2017, a storm caused the redoxcline to shift downward between lander deployments which were three days apart, causing a large difference in oxygen concentrations between deployments 1 and 2 (Table 1; Supplementary Fig. 2, Appendix 2). Stations D, E, and F were situated at depths below the halocline at all times (Fig. 1b). In 2016, bottom waters at the deeper stations E and F had O<sub>2</sub> concentrations of 7-30 μM, indicative of a recent MBI. In the two subsequent years, oxygen levels dropped and bottom waters were anoxic (<0.5 μM; the detection limit of the oxygen optodes attached to the lander) at station E in 2018 and station F in both 2017 and 2018. Station D (located closer to the halocline) was anoxic in 2016 and 2018 but had an O<sub>2</sub> concentration of ~8 μM in 2017 (Table 1). Note that the concentrations measured by the oxygen optodes on the lander are consistently lower than the values measured in the water column (Fig. 1c). This likely reflects spatial differences between concentrations in the water column at station BY15 and concentrations measured near the seabed.

#### 3.2 Sediment parameters

Solid-phase density showed no trend with sediment depth at any of the four sites, so values are reported as depth-averaged values. The shallow site (A) had a slightly higher solid-phase density ( $2.2 \pm 0.4 \text{ g cm}^{-3}$ ), compared to the deeper stations (D:  $1.9 \pm 0.4 \text{ g cm}^{-3}$ ; E:  $2.0 \pm 0.3 \text{ g cm}^{-3}$ ; F:  $1.9 \pm 0.5 \text{ g cm}^{-3}$ ). The solid-phase density recorded at the deeper stations is lower than that of typical siliclastic marine sediments (~2.6 g cm<sup>-3</sup>; Burdige, 2006), and this is partially explained by the high organic matter content (see below), which has a solid-phase density close to 1.0 g cm<sup>-3</sup>.

Porosity at station A had a distinct minimum (~0.4) at 2.5 cm depth before increasing again with depth (Fig. 2a). This profile suggests that at station A, a shallow layer (3-4 cm) of recent sediment overlies an old, consolidated clay layer. The recent sediment contains more sandy particles, which explains the lower porosity in the upper 4 cm. The porosity depth profiles at the three deeper sites (D, E, and F) were similar, with high values (> 0.9) in the upper three centimetres (Fig. 2b-d), gradually declining to ~0.8 in the deeper sediment layers. The apparent



constant porosity in the upper 3 cm of the sediment is most likely due to mixing of the fluffy upper layer during core sampling. The exponential decrease of porosity with depth is consistent with what is often encountered in coastal and shelf sediments (Boudreau et al., 1998).

At the shallowest station (A), the Al/Ti molar ratio (a proxy for the input of detrital material) of the sediment layers below 4 cm reflected the Al/Ti ratio of the average upper crust (34.8 mol/mol; McLennan, 2001) (Fig. 2e). However, above 4 cm, the Al/Ti ratio was markedly higher. Since Ti associates mainly with organic matter (Kryc et al., 2003), the elevated Al/Ti ratio of the upper sediment layer at station A is consistent with the selective removal of fine-grained organic-rich particles from erosion-transport bottoms. At the deeper sites (D, E, and F), Al/Ti molar ratios were close to the average ratio of the upper continental crust (McLennan, 2001) and did not show variation with depth or across sites. As parent soils or rocks are typically characterized by specific Al/Ti fingerprints, the consistency in Al/Ti ratio between stations D, E and F (Fig. 2f-h) suggests that these sites receive a similar type of detrital input.

The POC content was markedly higher in the deeper stations (D, E, and F) than in the shallow shelf station (A) (Fig. 2i-l). This is consistent with station A being an erosion-transport bottom, where most of the fine-grained POC particles are washed away, to finally accumulate in the deeper stations (Carman and Cederwall, 2001; Nilsson et al., 2018).

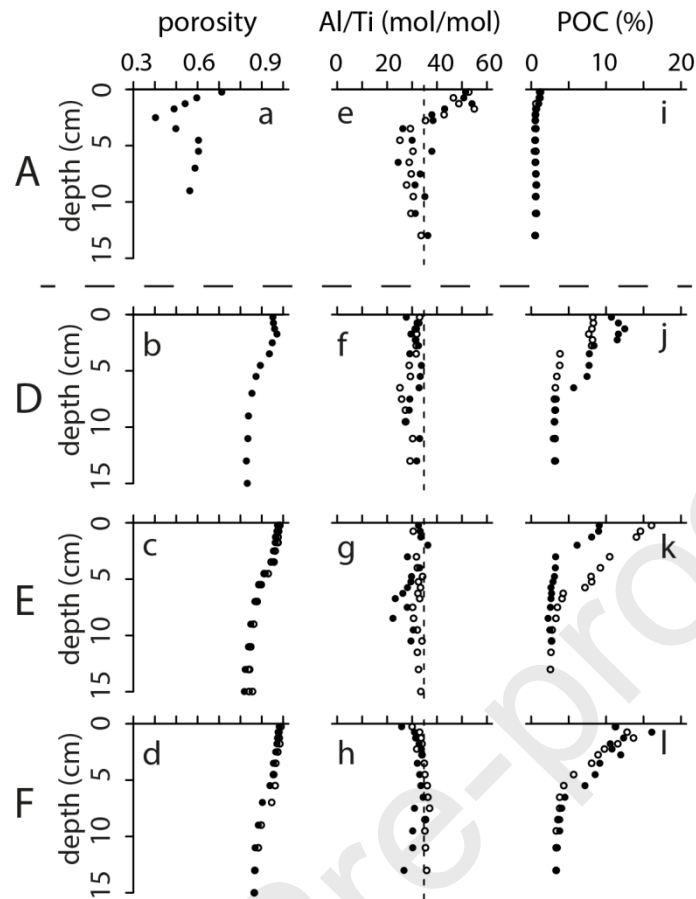


**Figure 2:** General sediment characterisation at the four sites (A, D, E, F). (a)-(d) Porosity depth profiles. Closed symbols are porosity values from April 2016 (this study), empty symbols are from 2015 (Hall et al., 2017). (e)-(h) Solid phase Al/Ti molar ratios at all sites recorded in April 2016. Open and closed symbols represent duplicate cores. The dashed line represents the average molar Al/Ti ratio of the upper continental crust (McLennan, 2001). (i)-(l) Particulate organic carbon (POC) concentrations in the sediment in April 2016. Open and closed symbols represent duplicate cores.

### 3.3 Solid-phase chemistry

Elemental concentrations (X) were normalized to Al, thus correcting for variations in the magnitude of detrital input (Fig. 3). The X/Al ratios in the upper 4 cm of the shallow station (A) were depleted (apart from Cd and U) relative to the sediment layers deeper than 4 cm, and generally lower than the average crustal value. Tungsten was consistently offset compared to the average crustal value, so we defined a local baseline (defined as the W/Al value of the sediment layers below 4 cm depth of station A; Fig. 3). At stations D, E and F, the X/Al ratios tended to be higher than the average crustal value, suggesting an enrichment in the deeper stations relative to the detrital input. Fe was enriched above the average crustal value over the

whole core depth at all deep stations ( $\text{Fe}/\text{Al} \sim 1.7$  times the average crust), while Mn showed only a strong enrichment at the deepest station F ( $\text{Mn}/\text{Al} \sim 2.7$  times the average crustal value). All trace elements examined (Co, Cd, Ni, Mo, As, W, V, and U) showed a stronger enrichment in the top 6 cm compared to the deeper sediment layers of the same core. Tungsten showed the strongest enrichment at the deepest station (F). The average sediment accumulation rate for the deep basin of the EGB is  $\sim 0.1 \text{ cm yr}^{-1}$  (Hille et al., 2006), and so the 6 cm depth horizon appears to correspond to the onset of persistent anoxia and euxinia in the area in 1955-1974 (Carstensen et al., 2014).

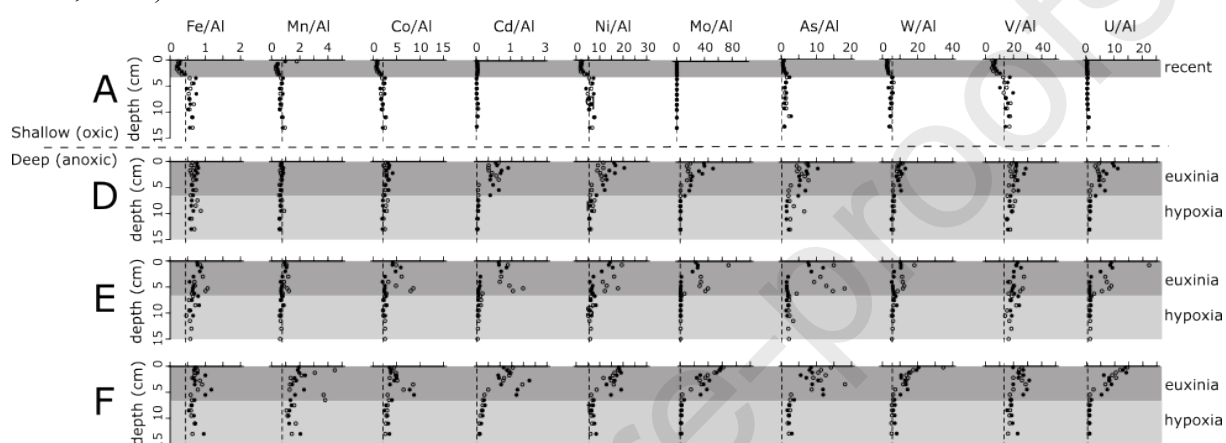


**Figure 3:** Depth profiles of X/Al ratios in sediments. Units are g/g for Fe/Al,  $10^{-2}$  g/g for Mn/Al and  $10^{-4}$  g/g for Co/Al, Cd/Al, Ni/Al, Mo/Al, As/Al, W/Al, V/Al, and U/Al. The dashed line represents the X/Al ratio of the average upper crust (McLennan, 2001), apart for Tungsten, where we defined a local baseline ( $\text{W}/\text{Al}=7 \cdot 10^{-4}$  g/g). Dark gray shading in station A panels represents the recent sediment (station A is an erosion-transport bottom and accumulates very little material). The dark gray shading in stations D, E and F corresponds to sediments accumulated since the onset of deep-water euxinia in the deeper Baltic Proper ( $\sim 1955-1974$ ), while light gray shading represents the antecedent period of deep-water hypoxia ( $[\text{O}_2] < 62.5 \mu\text{M}$ ; from  $\sim 1906$ ) (Carstensen et al., 2014). Open and closed symbols represent duplicate cores.

### 3.4 Water-column chemistry

Water column depth profiles of dissolved and suspended fractions were recorded in 2017. Dissolved Fe, Ni, and U (dFe, dNi and dU) showed little variation with depth (Fig. 4a,i,s). Consistent with previous observations (Hermans et al., 2019), concentrations of dMn were elevated near the seafloor (Fig. 4c). Concentrations of dCd, dMo and dAs were relatively constant over the first 50 m of the water column, below which concentrations gradually increased (Fig. 4g,k,m). Dissolved V gradually decreased with depth (Fig. 4q). The particulate fraction of Fe showed a peak at  $\sim 130$  m water depth (Fig. 4b). In contrast, the particulate

fraction of Mn and trace elements showed a higher concentration at greater depth (Fig. 4d,f,h,j,l,n,p,r,t).

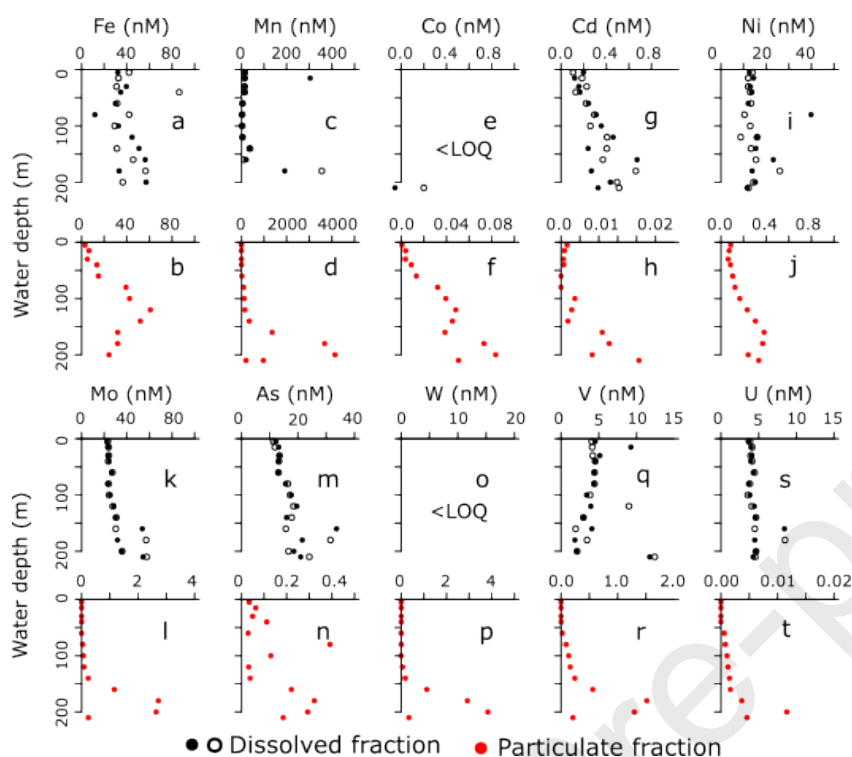


**Figure 4:** Water column depth profiles of dissolved ( $< 0.45 \mu\text{m}$ ) and particulate ( $> 0.45 \mu\text{m}$ ) fractions of (a),(b) Fe; (c),(d) Mn; (e),(f) Co; (g),(h) Cd; (i),(j) Ni; (k),(l) Mo; (m),(n) As; (o),(p) W; (q),(r) V; (s),(t) U. Samples were collected at site F (water depth = 210 m) in April 2017. Closed and open symbols represent duplicate samples for the dissolved fraction. Dissolved concentrations of Mo, U, V and W have been normalised to salinity. Concentrations for elements below the Limit of Quantification are marked as <LOQ.

### 3.5 Pore water chemistry

Both dFe and dMn showed elevated concentrations in the upper 3-4 cm of the shallow station (A) (Fig. 5), consistent with Fe and Mn cycles sustained by sediment mixing by burrowing fauna and oxygenated overlying water (Aller, 1990; Thamdrup et al., 1994a; van de Velde and Meysman, 2016). Note that in 2016, dFe was undetectable in the pore water at station A, though this was likely due to the methodological problem. At the deeper stations, dFe was only present in low concentrations near the sediment-water interface, and undetectable below the sulphide appearance depth (the dashed line in Fig. 5; data taken from Marzocchi et al., 2018). In contrast, dMn accumulated in the pore water of all stations after the inflow of oxygenated water (2017

for D, 2016 for E and F; Fig. 1c). The concentrations decreased with time, indicating that dMn was either redistributed through the sediment column and/or removed via precipitation (Fig. 5).

At station A, the pore water concentration of dCo correlated with dFe (Fig. 5), while dCd showed no trend with depth (Fig. 5). In the deeper stations, dCo and dCd only accumulated near the sediment-water interface, except for dCo in 2018 at station D. (Fig. 5). The dCd concentrations at the sediment-water interface increased with water depth (Fig. 5). Pore water profiles of dNi did not show any trend with sediment depth in any of the stations (Fig. 5). In 2018, the concentrations of dCo and dNi were highest at station D, similar to dMn (Fig. 5).

The pore water concentrations of dMo and dAs peaked at ~4 cm in the shallow station A, below the depth of Fe and Mn oxide reduction (Fig. 5). In the deeper stations, dAs and dMo were enriched near the sediment-water interface, and decreased with sediment depth (Fig. 5). Dissolved W, dV and dU did not accumulate in the pore water of station A (Fig. 5). In the deeper stations, dW and dV appeared to respond to the oxygenation events in the same way as dMn (Fig. 5). In contrast, dU concentrations showed increasing trends with station water depth, similar to dCd (Fig. 5).

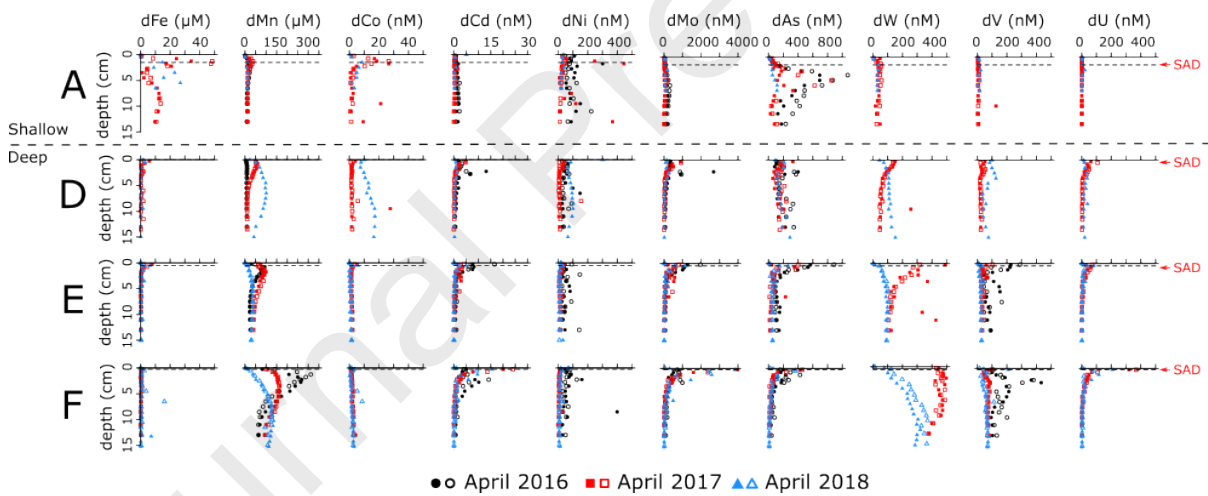


**Figure 5:** Pore water depth profiles recorded at stations A (water depth = 60 m, top row), D (water depth = 130 m, second row), E (water depth = 170 m, third row) and F (water depth = 210 m, bottom row) in April 2016, April 2017 and April 2018. Depth profiles from two replicate cores are shown (closed and open symbols). Black dashed line indicates depth where dissolved sulphide started accumulating (Sulphide Appearance Depth; SAD) in 2016 (depths were identical in 2017, except for station D where it was ~0.1 cm; Marzocchi et al., 2018).

### 3.6 Benthic fluxes

Sedimentary effluxes are reported as positive fluxes while sedimentary uptake are reported as a negative flux. Benthic fluxes from the shallow station A, which had a fully oxygenated water column, did not vary between sampling times for any of the redox-sensitive elements (Table 2). Fluxes of dFe and dMn measured at this station fell within the range of previously *in situ* measured fluxes of dFe and dMn in continental margin sediments underlying fully oxygenated bottom waters (Table 2). The fluxes of the other trace elements were a few orders of magnitude lower than the fluxes of dFe and dMn, and were found to be in the same range as previously measured fluxes in the a range of sediments, although dAs fluxes were slightly elevated compared to previously reported values from the Venice Lagoon (Table 2).

**Table 2:** Recorded range of significant fluxes at the oxic station (A) compared to fluxes found in the literature. All significant fluxes are reported in Supplementary Table 4. BW = bottom water.

Year	BW O <sub>2</sub> (μM)	Flux range (μmol m <sup>-2</sup> d <sup>-1</sup> )				
		Fe	Mn	Co	Cd	Ni
2016	340	+80	+26 – +28	-	-	+1.1 – +1.2
2017	110	+18	+12 – +35	-	-0.06 – +0.02	+1.1
	300	-	+14 – +34	-	-0.02	-2.6
2018	340	-	+50 – +110	-	-	+0.4 – +1.3
	340	+17	+6 – +112	-	-	+0.7 – +3.0
<i>Literature range</i>		-0.2 – +568 <sup>1-6</sup>	+3 – +1300 <sup>2,3,7,8</sup>	-	+0.013 – +0.05 <sup>9,10</sup>	+0.209 <sup>10</sup>

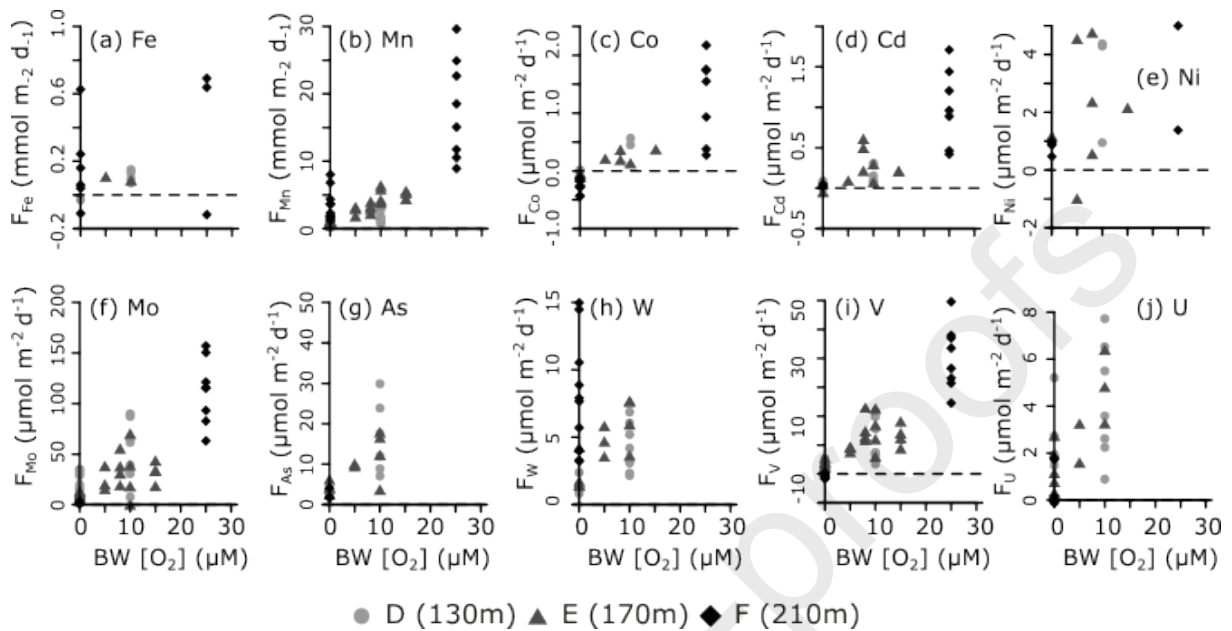
  

Year	BW O <sub>2</sub> (μM)	Flux range (μmol m <sup>-2</sup> d <sup>-1</sup> )				
		Mo	As	W	V	U
2016	340	+0.8 – +2	-	-	+0.2 – +0.4	-
2017	110	-	+1.5	-	+0.3 – +0.7	-0.03
	300	-	-	-0.55	-	-
2018	340	-	+0.3 – +0.5	+0.8	+0.2 – +0.3	+0.03 – +0.04
	340	+0.2 – +2	-	+0.2 – +0.5	+0.4 – +0.5	+0.2
<i>Literature range</i>		-1.66 – +1.22 <sup>9</sup>	-0.04 – +0.06 <sup>9</sup>	-	-2.0 – +0.31 <sup>9</sup>	-7.5 – +20.4 <sup>11</sup>

<sup>1</sup>(Elrod et al., 2004), <sup>2</sup>(Pakhomova et al., 2007), <sup>3</sup>(Almroth et al., 2009), <sup>4</sup>(Severmann et al., 2010), <sup>5</sup>(Noffke et al., 2012), <sup>6</sup>(Lenstra et al., 2018), <sup>7</sup>(Thamdrup et al., 1994b), <sup>8</sup>(Berelson et al., 2003), <sup>9</sup>Venice Lagoon (Turetta et al., 2005), <sup>10</sup>Gullmarsfjorden (Sundby et al., 1986; Westerlund et al., 1986), <sup>11</sup>(Point et al., 2007).

In the deeper stations (D-F), dFe, dMn, dV, dMo, dU, dCo, dCd, and dAs responded in a consistent way to the transient oxygenation event. The highest benthic effluxes were measured when the bottom water oxygen concentrations were the highest, and lower fluxes were measured during the anoxic periods (Fig. 6). Notable exceptions are the dMn and dW fluxes which remained relatively elevated at station F after return to anoxia. The fluxes of dFe and

dNi furthermore showed substantial variability, although higher fluxes of dNi were generally found at intermediate oxygen concentrations.



**Figure 6:** *In situ* measured trace element fluxes at the deeper stations (D, E, F) versus *in situ* measured bottom water  $O_2$  concentration (as reported in Table 1). Note that duplicate lander deployments have now been split up (bottom water  $O_2$  concentrations varied between deployments). Only statistically significant fluxes are shown (see section 2.2). All significant fluxes are reported in Supplementary Table 4.

#### 4. DISCUSSION

The deeper stations (D-F) of the EGB are long-term anoxic, but experienced a transient oxygenation in 2015 (stations E and F) and 2016 (station D) (Fig. 1c). Following these oxygenation events, trace element effluxes were generally higher than during bottom water anoxia (Fig. 6). The exposure of long-term anoxic sediments to oxygenated bottom water can lead to an increase in benthic effluxes via two mechanisms (see e.g. Scholz et al., 2011). Firstly, oxygenation of the bottom water can lead to the formation of metal (hydr)oxide minerals in the water column, which sink out and settle onto the sediment surface. Within the sediment, these metal (hydr)oxides become subsequently reduced, thus leading to a transient increase in the benthic release. Secondly, penetration of oxygen into the sediment can lead to oxidation and dissolution of authigenic minerals previously formed under anoxic bottom water conditions. In



the first case, the increased efflux is caused by the *reduction of oxidised minerals*, following an increase in trace element supply to the sediment, leading to enhanced sedimentary recycling of the element (this typically occurs at the sediment-water interface). In contrast, in the second case, the increased benthic efflux is caused by *oxidation of reduced minerals* in the sediment, and in this way, elements that would be otherwise buried are now remobilised. Therefore, we propose to name the first mechanism (reduction in the sediment) ‘**enhanced elemental recycling**’. For the second mechanism (oxidation in the sediment) we propose ‘**oxidative remobilisation**’. Whether a particular element shows a higher benthic efflux due to enhanced elemental recycling or oxidative remobilisation depends on its redox and adsorption properties.

It is difficult to distinguish between the two mechanisms based on benthic flux data alone, as both mechanisms will lead to higher effluxes after the inflow of oxygen. Additionally, they will both lead to accumulation of solutes in the pore water after dissolution of either the Fe or Mn oxide carrier or the authigenic mineral. To distinguish between the mechanisms, we can compare the element-to-aluminum ratio (X/Al) of the suspended particles in the water column with the X/Al ratio of the upper few centimetres of the sediment column. If the X/Al ratio in the water column is higher than the X/Al ratio of the sediment, the particulate input to the sediment of the element in question is higher after the inflow compared to before the inflow. The higher input to the sediment is then likely the consequence of the inflow of oxygenated water and suggests enhanced elemental recycling. In the case of oxidative remobilisation, one would expect a decrease in X/Al ratio of the sediment (since authigenic minerals in the sediment are being dissolved), with the X/Al ratio of the detrital input being the minimum value. However, the X/Al ratio in the water column would also be lower, since no new reduced authigenic minerals are formed in the water column. The X/Al composition of the water column would then be expected to reflect the ratio of the detrital input. Thus, if the X/Al ratio of the water column is comparable to or lower than the X/Al of the sediment, the enhanced benthic release is likely related to oxidative remobilisation. This approach assumes that there was no significant recycling in the sediment after deposition under anoxic conditions because the X/Al ratio in the water column would then always be higher than in the sediment. Since the EGB was euxinic before the inflow (Sommer et al., 2017), one expects a limited recycling of elements that form sulphides (i.e. Fe, Co, Cd, Ni) or of elements that are retained under euxinic conditions (Mo, As, W, V, U). We therefore believe that the comparison of metal-to-aluminum ratios can give us some insight into the exact source of the measured flux.

#### 4.1 Major carrier phases: Fe and Mn

During an inflow of oxygenated water, Fe and Mn are expected to form oxides in the water column, sink to the sediment, experience reduction and be released back to the water column as soluble  $\text{Fe}^{2+}$  and  $\text{Mn}^{2+}$ . These reduced species are then re-oxidised again, leading to higher X/Al ratios in the water column (Sulu-gambari et al., 2017; Hermans et al., 2019). Indeed, both Fe and Mn had a higher X/Al ratio in the water column than in the sediment (Fig. 7). For Fe however, the higher ratios in the water column also persisted after the water column had turned anoxic again at station F in 2017, indicating the ventilation was muted in the deepest part of the basin. This is consistent with the observed dFe fluxes, which are of a similar magnitude for sediments underlying anoxic and hypoxic water columns (Fig. 6a). Iron did show higher benthic fluxes after the inflow (Fig. 6a), but the increase was limited to  $\sim +0.6 \text{ mmol m}^{-2} \text{ d}^{-1}$ , which is comparable to dFe fluxes observed in San Pedro basin sediments underlying low-oxygen bottom waters ( $\sim +0.6 \text{ mmol m}^{-2} \text{ d}^{-1}$ ; Severmann et al., 2010).

In contrast, Mn showed much higher water column X/Al ratios at stations D and E (hypoxic in 2017), and the dMn fluxes had increased to  $+30 \text{ mmol m}^{-2} \text{ d}^{-1}$  (Fig. 6b), which was three orders of magnitude higher than those before the MBI ( $+7.1 - +8.2 \text{ } \mu\text{mol m}^{-2} \text{ d}^{-1}$ ; Neretin et al., 2003). Generally, distinct Mn carbonates sedimentary layers in Baltic Sea sediments have been found to correspond to (long-lasting) inflows of oxygenated water (Huckriede and Meischner, 1996; Neumann et al., 1997; Sternbeck and Sohlenius, 1997; Neumann et al., 2002; Scholz et al., 2013). During short-lived inflow events, however, Mn carbonate formation is limited (Heiser et al., 2001). Indeed, we found that dMn accumulated in the pore water after the inflow of oxygenated water (Fig. 5), indicating that very little Mn was retained in the sediment as e.g. Mn-rich carbonate minerals. This is consistent with the limited solid-phase enrichments (Fig. 3) and previous observations from the 2015 inflow event (Scholz et al., 2018; Dellwig et al., 2018). Our results support the hypothesis of Hermans et al. (2019), who suggested that high concentrations of suspended Mn oxides observed in the deep waters of the basin could be caused by enhanced Mn recycling due to the absence of an efficient sink in the sediments of the western flank of the EGB.

Before the MBI event, the dFe concentrations in the water column were 10 to 15 times lower than the dMn concentrations (Fig. 4a-d; Hermans et al., 2019), and so it was expected that the

dFe efflux would be smaller than the dMn efflux after the inflow. Indeed, just after the inflow (in 2016), the measured dMn flux at station F was 30 times higher than that of dFe (Fig. 6a,b). The release of dFe to the water column was likely further limited by the formation of insoluble FeS in the sediment. Iron sulphide formation is supported by the pore water profiles of dFe, which show no accumulation in any of the deep stations (Fig. 5). Based on the bottom water concentration ratio between dMn and dFe, the enhanced release of dFe (without any trapping) should be 10-15 times smaller than the dMn flux, i.e.  $+1.2 - +1.8 \text{ mmol m}^{-2} \text{ d}^{-1}$ . However, only  $+0.6 \text{ mmol m}^{-2} \text{ d}^{-1}$  was released, which indicates that 50-70% of the dFe was trapped as FeS. This highlights the role of free sulphide as a very efficient Fe trap, consistent with the close correlation between Fe and S in the solid phase of the EGB and other deep basins in the Baltic Sea (Suess, 1979; Sternbeck and Sohlenius, 1997; Scholz et al., 2013; Dijkstra et al., 2016).

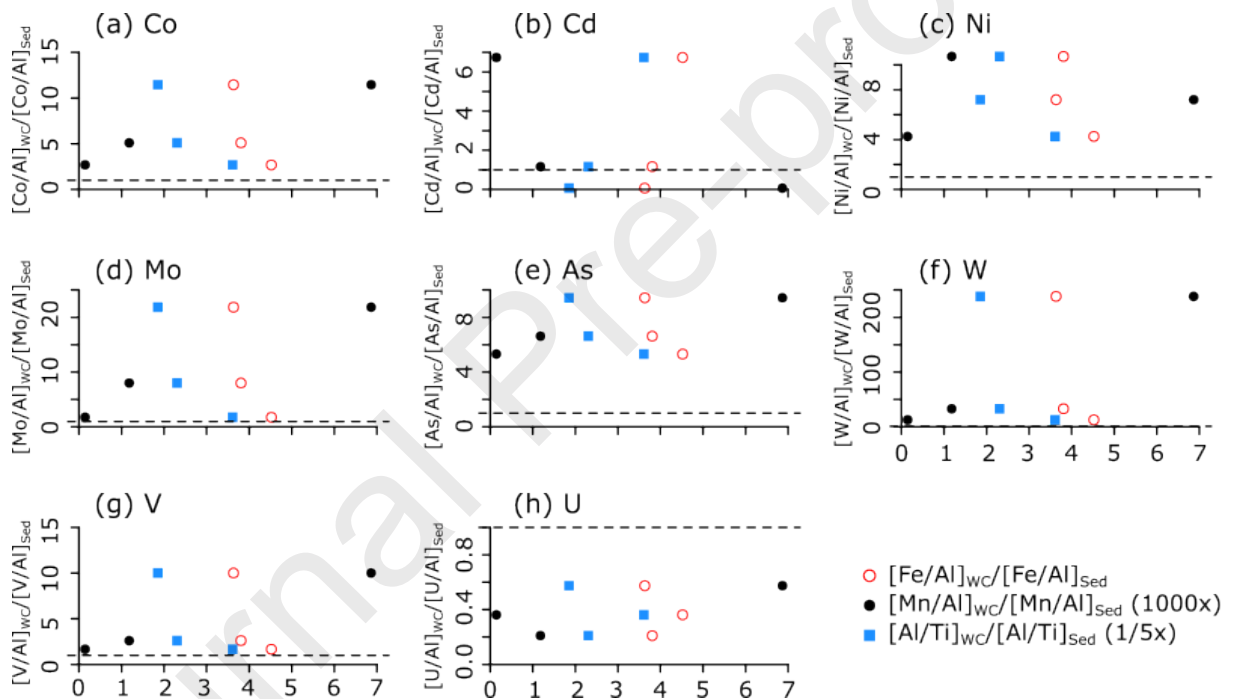


**Figure 7:** Correlation between water column enrichments relative to sediment enrichments (calculated as the metal-to-aluminum ratio of the water column relative to the metal-to-aluminum ratio of the sediment;  $[X/Al]_{wc}/[X/Al]_{sed}$ ) of each of the trace elements studied versus the water column enrichments of Fe (hollow red circles), Mn (filled black circles) and Ti (filled blue squares) for stations D, E and F. The dashed line indicates 1, values plotted below this value show depletion in the water column, values above this line are enriched in the water column.

#### 4.2 Divalent cations (Co, Cd and Ni)

The divalent cations (Co, Cd and Ni) can adsorb onto Fe or Mn oxides (Gendron et al., 1986; Kay et al., 2001), but are also particle-reactive and hence can adsorb on other carrier phases as well, like organic matter or clays (O'Connor and Kester, 1975; Sheng et al., 2004; Vijayaraghavan et al., 2005). Dissolved Co and dCd showed higher fluxes right after the inflow

(Fig. 6c,d), whereas this trend was less obvious for dNi due to high scatter in the data (Fig. 6e). The water column enrichment of Co correlated positively with that of Mn (Fig. 7a), indicating that Co adsorption to, or incorporation of Co in Mn oxides (Lee and Tebo, 1994; Moffett and Ho, 1996), drove the input of Co to the sediment. The enhanced release of dCo after the inflow was thus likely caused by the enhanced input of Mn oxide minerals to the sediment and the subsequent reductive dissolution of the carrier phase. After the inflow, dCo did not accumulate in the pore water (apart from one observation at station D in 2018; Fig. 5), indicating that some of the Co was retained in the sediment, likely due to incorporation in FeS minerals (Wallmann, 1992; Saito and Moffett, 2002). When the water column returned to anoxia, Co was taken up by the sediment (Fig. 6c), probably due to co-precipitation with sulphide minerals (Wallmann, 1992).

Water column enrichments of Cd showed an inverse correlation with Mn and seemed to correlate better with Fe or Ti (indicative of detrital material) (Fig. 7b). This could suggest that Cd preferentially adsorbs on Fe oxides rather than on Mn oxides, although it is known to adsorb on both (Gadde and Laitinen, 1974). Alternatively, it could indicate that Cd transport to the sediment was preferentially controlled by detrital input and potential adsorption on clay (Suraj et al., 1998), rather than on Fe or Mn (hydr)oxides. The Cd/Al ratio in the water column was generally lower than or similar to the Cd/Al ratio in the sediment of the stations that were hypoxic in 2017 (D and E) (Fig. 7b). This similarity suggests that Cd likely experienced oxidative remobilisation, rather than an enhanced input and recycling. Cadmium is indeed known to be susceptible to remobilisation following re-exposure to oxygen (Westerlund et al., 1986; Tribovillard et al., 2006). Interestingly, the dCd pore water profile in 2016 at station F showed a peak well below the sulphide appearance depth, which could be caused by dCd release following the dissolution of an oxide carrier phase (Fig. 5). At this station, the Cd/Al enrichments in the water column were also higher than in the sediment (Fig. 7b). Dissolved Cd concentrations in the water column increased with water depth, which could lead to differences in adsorption capacity. Overall, the response of Cd to re-oxygenation seems to differ between stations and is likely very dependent on local conditions.

Benthic dNi fluxes did not show a clear trend with oxygen concentration (Fig. 6e), nor did the water column enrichment seem to correlate with Fe, Mn or Ti (Fig. 7c). Potentially, Ni transport is predominantly controlled by adsorption on organic compounds, rather than on Fe or Mn oxides (Vijayaraghavan et al., 2005). Additionally, Ni is less likely to experience

oxidative remobilisation and should therefore serve as a good indicator of primary production, as previously reported (Tribovillard et al., 2006; Böning et al., 2015). Overall, our data suggest that Ni was not very sensitive to the transient re-oxygenation event.

### 4.3 Metalloids (Mo, As and W)

All three metalloids (Mo, As and W) showed higher benthic effluxes when the water column was oxygenated (Fig. 6f,g,h). After the return to anoxia, however, dMo and dAs fluxes rapidly decreased, while dW fluxes remained high (Fig. 6h). This indicates that all three elements have a similar response to oxygenation, but show a divergent response when anoxia returns.

Molybdenum enrichments in the water column correlated well with Mn enrichments (Fig. 7d), consistent with previous observations of the relation between formation of Mn oxides in the water column and the delivery of Mo to the sediment (Berrang and Grill, 1974; Scholz et al., 2013; Sulu-Gambari et al., 2017). However, the benthic dMo fluxes rapidly decreased when the water column returned to anoxia (Fig. 6f), while dMn fluxes remained high (Fig. 6b). Additionally, Mo did not accumulate much in the pore water (Fig. 5). These factors indicate that a fraction of the Mo was retained in the sediment, potentially sequestered by organic matter within the sulfidic zone (Scholz et al., 2018). Our observations hence agree with a recent study by Scholz et al. (2018) on the impact of the MBI on Mo cycling in the Gotland Basin.

Overall, the As cycle was highly similar to that of Mo following the transient re-oxygenation. Water column enrichments correlated closely with Mn (Fig. 7e), fluxes rapidly decreased after the return to anoxia (Fig. 6e) and accumulation in the pore water was limited to the sediment-water interface (Fig. 5). This again suggests an enhanced delivery to the sediment via adsorption on oxide minerals, followed by retention of a fraction of the As in the euxinic sediment, likely sequestered in iron-sulphide minerals (Huerta-Diaz and Morse, 1992).

Immediately following the transient oxygenation, W responded similarly to Mo and As. Water column enrichments correlated with Mn enrichments (Fig. 7f), consistent with the adsorption of W on Mn oxides (Gustafsson, 2003; Dellwig et al., 2019). However, after the dissolution of the oxides in the sediment, W accumulated in the pore water (Fig. 5) and benthic fluxes remained high after return to anoxic conditions (Fig. 6h). The lack of efficient trapping in anoxic conditions, and the lack of a downward flux in the pore water (Fig. 5) suggests that very little – if any – W was retained in the sediment. The latter could be caused by the formation

of thioesters in the sulphidic pore water, which reduce the adsorption capacity of the W complex (Cui and Johannesson, 2017).

#### 4.4 Vanadium

In oxygenated conditions, V is particle reactive and can adsorb onto Fe or Mn oxides (Wehrli and Stumm, 1989b), which is evident from the correlation between the water column enrichment of V and Mn (Fig. 7g). The enhanced benthic fluxes of V after the inflow event (Fig. 6i) are thus likely related to an enhanced sedimentary deposition of V associated with Mn oxides, which has been proposed earlier by Scholz et al. (2013). Pore water accumulation of V was limited (Fig. 5), and V fluxes rapidly decreased when the bottom waters returned to anoxia (Fig. 6i). This indicates that at least a fraction of the V that entered the sediment adsorbed on oxide minerals was retained (Scholz et al., 2013). The retention of V is driven by the reduction from its V(V) form to its V(IV) or V(III) forms under reducing conditions. The reduced forms of V can either form insoluble oxide or hydroxide phases, or adsorb on particles (Emerson and Husted, 1991; Wanty and Goldhaber, 1992).

#### 4.5 Uranium

In its oxidised form, U can adsorb on Fe or Mn oxides (Waite et al., 1994; Wang et al., 2013). However, the U/Al ratios in the water column were consistently lower than in the sediment, and there was no correlation with Fe, Mn, or Ti (Fig. 7h). The lack of enrichment in the water column indicates that the enhanced benthic fluxes after the oxygenation event (Fig. 6j) were most likely related to oxidative remobilisation. Pore water profiles of dU showed a concentration peak at the sediment-water interface (Fig. 5), which suggests that dU was released due to the oxidative dissolution of authigenic U minerals. Uranium is known to be susceptible to remobilisation following re-exposure to oxygen (Anderson et al., 1989; Barnes and Cochran, 1990).

The source for U is authigenic minerals that had been formed in the upper 3 mm of the sediment of stations D, E, and F before the MBI. Most likely, the measured fluxes represent a combination of dissolution of authigenic minerals and elements released during the mineralisation of organic matter. Nevertheless, the measured dU fluxes were consistently higher after the inflow of oxygenated water, suggesting that authigenic minerals were being dissolved. In contrast to Zheng et al. (2002), who reported a threshold oxygen level of 15  $\mu\text{M}$  above which U remobilisation occurs, our results show that even a limited transient increase of



oxygen can lead to measurable losses of U from the sediment. For instance, in 2017, the bottom water oxygen concentration at station E was  $< 10 \mu\text{M}$ , while the benthic dU flux reached  $\sim +4 \mu\text{mol m}^{-2} \text{d}^{-1}$ . This is more than twice the flux measured when station E returned to anoxia in 2018 (Fig. 6j).

#### 4.6 Wider implications for oxygenation and trace nutrient fertilisation

Primary productivity is limited by the availability of Fe and other trace elements in large regions of the ocean (Mahowald et al., 2018; Baeyens et al., 2018). Sediments underlying an oxic water column generally release a fraction of the reactive Fe, Mn and trace elements that are deposited in solid forms (as shown by the predominantly positive fluxes in Table 2), and are thus likely a significant source of these elements (Elrod et al., 2004; Severmann et al., 2010; Dale et al., 2015). In contrast, sediments underlying a euxinic water column release a much smaller fraction (if any) of the trace element input they receive, in particular for elements that form sulphide minerals or get incorporated in FeS minerals, and thus act as permanent sinks for Fe and other trace elements. Changes in the oxygenation state of the water column can therefore have important consequences for the ocean's trace element inventory.

A clear example of this is the oxygen minimum zone in the Peru upwelling system. Over the past 140,000 years, iron limitation has been shown to limit denitrification during times when the oxygen minimum zone has been larger, due to efficient sedimentary retention of Fe under more strongly reducing conditions (Scholz et al., 2014). As a result of increasing climate change, oxygen minimum zones are expected to expand in the coming decades (Keeling et al., 2010). It is thus plausible that the euxinic sink for Fe and other trace elements will increase over time (Scholz et al., 2014). Our results here indicate that the transient re-oxygenation of a euxinic system leads to enhanced delivery of Fe, Mn, and trace elements to the sediment. After re-establishment of anoxia, Mn and W are readily recycled to the water column, but at least fractions of Fe, Co, Mo, As, and V are retained in the sediment. Hence, while expanding the euxinic sink will lead to less recycling back to the water column, transient re-oxygenation of these euxinic systems will promote the long-term burial of Fe and other trace elements. This would decrease the ocean's trace element inventory even more, potentially further constraining primary productivity in regions where trace elements are limiting.



## 5. SUMMARY AND CONCLUSIONS

We have conducted *in situ* measurements of benthic dissolved element fluxes following transient oxygenation of long-term (~10 year) anoxic sediments. Our results indicate that the oxygenation event caused by an Major Baltic Inflow in the Eastern Gotland Basin increased the benthic effluxes of Fe, Mn, V, Mo, Co, W, and As via ‘enhanced elemental recycling’ – the sedimentary reduction of metal oxides formed in the water column. Uranium was released due to ‘oxidative remobilisation’ – the re-oxygenation of previously anoxic sediments, which leads to dissolution of authigenic minerals. The sedimentary release of Cd was strongly dependent on local conditions, and was found to be a result of both mechanisms. Nickel showed limited response to the transient oxygenation.

Our results suggest that the oxygenation event led to a transiently enhanced input of Fe, Mn, Co, Mo, As, W, and V into the sediment, predominantly modulated by the formation of Mn oxides in the water column. Iron oxides were less important as a carrier phase, most likely due to the limited presence of dFe in the water column before the inflow. Cadmium, Ni, and U were less strongly affected by water column oxide formation, and Cd and U were likely lost from the sediment because of oxidative dissolution of reduced minerals. After the transient input of Fe, Mn Co, Mo, As, W, and V, the oxides dissolved in the sediment. This lead to almost quantitative recycling of Mn and W to the water column. In contrast, a fraction of the Fe, Co, Mo, As, and V that entered the sediment were converted to sulphide minerals or formed insoluble reduced minerals, which lead to enhanced retention of these elements in the sediment after the re-establishment of anoxia.

Overall, our results suggest that transient re-oxygenation of a previously euxinic water column only has a transient effect on Mn or W, but promotes the burial of Fe, Co, Mo, As, and V. A climate change driven increase in the spatial extent of regions underlying euxinic water columns, in combination with transient re-oxygenation events, could potentially lead to more frequent transient re-oxygenation events. Over longer time scales, the resulting enhanced removal of Fe and other bio-essential trace elements from the water column via burial in the sediments could potentially lead to trace element limitation of primary production in regions where these euxinic zones develop.

## 6. ACKNOWLEDGEMENTS

The research leading to these results has received funding from the European Research Council under the European Union's Seventh Framework Programme (FP/2007-2013) through ERC Grant 306933 (FJRM), the Netherlands Organization for Scientific Research (VICI grant 016.VICI.170.072 to FJRM) and was financially supported by Research Foundation Flanders (PhD Fellowship to SVDV), the Belgian American Educational Foundation (post-doctoral Fellowship to SVDV), the European Union's Horizon 2020 research and innovation programme (Marie Skłodowska-Curie grant agreement No. 656385 to UM), and the Swedish Research Council (VR grant 2015-03717 to POJH). The authors would like to thank the crew of the University of Gothenburg R/V Skagerak for technical assistance.

## 7. References

- Aller R. C. (1990) Bioturbation and manganese cycling in hemipelagic sediments. *Philos. Trans. R. Soc. London A Math. Phys. Eng. Sci.* **331**, 51–68.
- Almroth E., Tengberg A., Andersson J. H., Pakhomova S. and Hall P. O. J. (2009) Effects of resuspension on benthic fluxes of oxygen, nutrients, dissolved inorganic carbon, iron and manganese in the Gulf of Finland, Baltic Sea. *Cont. Shelf Res.* **29**, 807–818.
- Anderson R. F., Lehuray A. P., Fleisher M. Q. and Murray J. W. (1989) Uranium deposition in saanich inlet sediments, vancouver island. *Geochim. Cosmochim. Acta* **53**, 2205–2213.
- Anderson T. F. and Raiswell R. (2004) Sources and mechanisms for the enrichment of highly reactive iron in euxinic Black Sea sediments. *Am. J. Sci.* **304**, 203–233. Available at: <http://eprints.whiterose.ac.uk/333/> [Accessed March 12, 2018].
- Baeyens W., Gao Y., Davison W., Galceran J., Leermakers M., Puy J., Superville P.-J. and Beguery L. (2018) In situ measurements of micronutrient dynamics in open seawater show that complex dissociation rates may limit diatom growth. *Sci. Rep.* **8**, 16125. Available at: <http://www.nature.com/articles/s41598-018-34465-w> [Accessed December 4, 2018].
- Barnes C. E. and Cochran J. K. (1990) Uranium removal in oceanic sediments and the oceanic U balance. *Earth Planet. Sci. Lett.* **97**, 94–101.
- Berelson W., McManus J., Coale K., Johnson K., Burdige D., Kilgore T., Colodner D., Chavez F., Kudela R. and Boucher J. (2003) A time series of benthic flux measurements from Monterey Bay, CA. *Cont. Shelf Res.* **23**, 457–481.
- Berrang P. G. and Grill E. V. (1974) The effect of manganese oxide scavenging on molybdenum in saanich inlet, British Columbia. *Mar. Chem.* **2**, 125–148. Available at: <https://www.sciencedirect.com/science/article/pii/0304420374900334> [Accessed July 3, 2019].
- Bertine K. K. (1972) The deposition of molybdenum in anoxic waters. *Mar. Chem.* **1**, 43–53.
- Blomqvist S., Ekeröth N., Elmgren R. and Hall P. (2015) Long overdue improvement of box corer sampling. *Mar. Ecol. Prog. Ser.* **538**, 13–21. Available at: <http://www.int-res.com/abstracts/meps/v538/p13-21/> [Accessed September 11, 2017].
- Böning P., Shaw T., Pahnke K. and Brumsack H.-J. (2015) Nickel as indicator of fresh organic matter in upwelling sediments. *Geochim. Cosmochim. Acta* **162**, 99–108. Available at: <https://www.sciencedirect.com/science/article/pii/S0016703715002331> [Accessed February 6, 2019].
- Boudreau B. P., Mucci A., Sundby B., Luther III G. W. and Silverberg N. (1998) Comparative diagenesis at three sites on the Canadian continental margin. *J. Mar. Res.* **56**, 1259–1284.
- Buck K. N., Lohan M. C., Berger C. J. M. and Bruland K. W. (2007) Dissolved iron

- speciation in two distinct river plumes and an estuary: Implications for riverine iron supply. *Limnol. Oceanogr.* **52**, 843–855. Available at: <http://doi.wiley.com/10.4319/lo.2007.52.2.0843> [Accessed July 9, 2019].
- Burdige D. J. (2006) *Geochemistry of Marine Sediments.*, Princeton University Press.
- Carman R. and Cederwall H. (2001) Sediments and Macrofauna in the Baltic Sea — Characteristics, Nutrient Contents and Distribution. In Springer, Berlin, Heidelberg. pp. 289–327. Available at: [http://www.springerlink.com/index/10.1007/978-3-662-04453-7\\_11](http://www.springerlink.com/index/10.1007/978-3-662-04453-7_11) [Accessed August 10, 2018].
- Carstensen J., Andersen J. H., Gustafsson B. G. and Conley D. J. (2014) Deoxygenation of the Baltic Sea during the last century. *Proc. Natl. Acad. Sci. U. S. A.* **111**, 5628–33. Available at: <http://www.ncbi.nlm.nih.gov/pubmed/24706804> [Accessed September 12, 2017].
- Cui M. and Johannesson K. H. (2017) Comparison of tungstate and tetrathiotungstate adsorption onto pyrite. *Chem. Geol.* **464**, 57–68. Available at: <https://www.sciencedirect.com/science/article/pii/S0009254116306441> [Accessed March 13, 2018].
- Cumberland S. A., Douglas G., Grice K. and Moreau J. W. (2016) Uranium mobility in organic matter-rich sediments: A review of geological and geochemical processes. *Earth-Science Rev.* **159**, 160–185. Available at: <https://www.sciencedirect.com/science/article/pii/S001282521630099X> [Accessed February 6, 2019].
- Dale A. W., Nickelsen L., Scholz F., Hensen C., Oeschies A. and Wallmann K. (2015) A revised global estimate of dissolved iron fluxes from marine sediments. *Global Biogeochem. Cycles* **29**, 1–17.
- Dellwig O., Schnetger B., Meyer D., Pollehne F., Häusler K. and Arz H. W. (2018) Impact of the Major Baltic Inflow in 2014 on Manganese Cycling in the Gotland Deep (Baltic Sea). *Front. Mar. Sci.* **5**, 248. Available at: <https://www.frontiersin.org/article/10.3389/fmars.2018.00248/full> [Accessed August 11, 2018].
- Dellwig O., Wegwerth A., Schnetger B., Schulz H. and Arz H. W. (2019) Dissimilar behaviors of the geochemical twins W and Mo in hypoxic-euxinic marine basins. *Earth-Science Rev.* **193**, 1–23. Available at: <https://doi.org/10.1016/j.earscirev.2019.03.017>.
- Dijkstra N., Slomp C. P. and Behrends T. (2016) Vivianite is a key sink for phosphorus in sediments of the Landsort Deep, an intermittently anoxic deep basin in the Baltic Sea. *Chem. Geol.* **438**, 58–72. Available at: <https://www.sciencedirect.com/science/article/pii/S0009254116302650> [Accessed June 26, 2019].
- Elrod V. A., Berelson W. M., Coale K. H. and Johnson K. S. (2004) The flux of iron from continental shelf sediments: A missing source for global budgets. *Geophys. Res. Lett.* **31**, 2–5.
- Emerson S. R. and Husted S. S. (1991) Ocean anoxia and the concentrations of molybdenum and vanadium in seawater. *Mar. Chem.* **34**, 177–196.
- Fitzsimmons J. N., John S. G., Marsay C. M., Hoffman C. L., Nicholas S. L., Toner B. M., German C. R. and Sherrell R. M. (2017) Iron persistence in a distal hydrothermal plume supported by dissolved–particulate exchange. *Nat. Geosci.* **10**, 195–201. Available at: <http://www.nature.com/articles/ngeo2900> [Accessed February 6, 2019].
- Gadde R. R. and Laitinen H. A. (1974) Heavy metal adsorption by hydrous iron and manganese oxides. *Anal. Chem.* **46**, 2022–2026. Available at: <http://pubs.acs.org/doi/abs/10.1021/ac60349a004> [Accessed July 3, 2019].
- Gendron A., Silverberg N., Sundby B. and Lebel J. (1986) Early diagenesis of cadmium and cobalt in sediments of the Laurentian Trough. *Geochim. Cosmochim. Acta* **50**, 741–747.
- GEOTRACES (2006) *GEOTRACES Science plan.*, Latimer Trend & Co Ltd, Plymouth. Available at: [http://www.geotraces.org/libraries/documents/Science\\_plan.pdf](http://www.geotraces.org/libraries/documents/Science_plan.pdf).
- Giménez J., Martínez M., de Pablo J., Rovira M. and Duro L. (2007) Arsenic sorption onto

- natural hematite, magnetite, and goethite. *J. Hazard. Mater.* **141**, 575–580.
- Gustafsson J. P. (2003) Modelling molybdate and tungstate adsorption to ferrihydrite. *Chem. Geol.* **200**, 105–115. Available at: <https://www.sciencedirect.com/science/article/pii/S000925410300161X> [Accessed March 13, 2018].
- Hall P. O. J., Almroth Rosell E., Bonaglia S., Dale A. W., Hylén A., Kononets M., Nilsson M., Sommer S., van de Velde S. and Viktorsson L. (2017) Influence of natural oxygenation of Baltic proper deep water on benthic recycling and removal of phosphorus, nitrogen, silicon and carbon. *Front. Mar. Sci.* **4**, 27.
- Hastings D. W., Emerson S. R. and Mix A. C. (1996) Vanadium in foraminiferal calcite as a tracer for changes in the areal extent of reducing sediments. *Paleoceanography* **11**, 665–678. Available at: <http://doi.wiley.com/10.1029/96PA01985> [Accessed March 12, 2018].
- Heiser U., Neumann T., Scholten J. and Stüben D. (2001) Recycling of manganese from anoxic sediments in stagnant basins by seawater inflow: a study of surface sediments from the Gotland Basin, Baltic Sea. *Mar. Geol.* **177**, 151–166. Available at: <https://www.sciencedirect.com/science/article/abs/pii/S0025322701001293> [Accessed July 1, 2019].
- Hermans M., Lenstra W. K., van Helmond N. A. G. M., Behrends T., Egger M., Séguret M. J. M., Gustafsson E., Gustafsson B. G. and Slomp C. P. (2019) Impact of natural re-oxygenation on the sediment dynamics of manganese, iron and phosphorus in a euxinic Baltic Sea basin. *Geochim. Cosmochim. Acta* **246**, 174–196. Available at: <https://www.sciencedirect.com/science/article/pii/S001670371830663X> [Accessed December 3, 2018].
- Hille S., Leipe T. and Seifert T. (2006) Spatial variability of recent sedimentation rates in the Eastern Gotland Basin (Baltic Sea). *Oceanologia* **48**, 287–307.
- Huckriede H. and Meischner D. (1996) Origin and environment of manganese-rich sediments within black-shale basins. *Geochim. Cosmochim. Acta* **60**, 1399–1413. Available at: <https://www.sciencedirect.com/science/article/pii/0016703796000087?via%3Dihub> [Accessed July 20, 2018].
- Huerta-diaz M. A. and Morse J. W. (1992) Pyritization of trace metals in anoxic marine sediments. *Geochim. Cosmochim. Acta* **56**, 2681–2702.
- Hylén A., van de Velde S., Ekeröth N. and Hall P. O. J. Evaluation flux measurements using in situ benthic landers. *Limnol. Oceanogr. Methods*.
- Jickells T. D. et al. (2005) Global iron connection between desert dust, ocean biogeochemistry, and climate. *Science (80- )*. **308**, 67–71.
- Jilbert T. and Slomp C. P. (2013) Iron and manganese shuttles control the formation of authigenic phosphorus minerals in the euxinic basins of the Baltic Sea. *Geochim. Cosmochim. Acta* **107**, 155–169. Available at: <http://dx.doi.org/10.1016/j.gca.2013.01.005>.
- Jones M. E., Beckler J. S. and Taillefert M. (2011) The flux of soluble organic-iron(III) complexes from sediments represents a source of stable iron(III) to estuarine waters and to the continental shelf. *Limnol. Oceanogr.* **56**, 1811–1823. Available at: <http://doi.wiley.com/10.4319/lo.2011.56.5.1811> [Accessed July 9, 2019].
- Kay J. T., Conklin M. H., Fuller C. C. and O'Day P. A. (2001) Processes of Nickel and Cobalt Uptake by a Manganese Oxide Forming Sediment in Pinal Creek, Globe Mining District, Arizona. *Environ. Sci. Technol.* **35**, 4719–4725.
- Keeling R. F., Körtzinger A. and Gruber N. (2010) Ocean Deoxygenation in a Warming World. *Ann. Rev. Mar. Sci.* **2**, 199–229. Available at: <http://www.annualreviews.org/doi/10.1146/annurev.marine.010908.163855> [Accessed December 4, 2018].
- Kirk M. F., Roden E. E., Crossey L. J., Brealey A. J. and Spilde M. N. (2010) Experimental analysis of arsenic precipitation during microbial sulfate and iron reduction in model aquifer sediment reactors. *Geochim. Cosmochim. Acta* **74**, 2538–2555. Available at: <https://www.sciencedirect.com/science/article/pii/S001670371000061X> [Accessed



- March 13, 2018].
- Klar J. K., Homoky W. B., Statham P. J., Birchill A. J., Harris E. L., Woodward E. M. S., Silburn B., Cooper M. J., James R. H., Connelly D. P., Chever F., Lichtschlag A. and Graves C. (2017) Stability of dissolved and soluble Fe(II) in shelf sediment pore waters and release to an oxic water column. *Biogeochemistry* **135**, 49–67. Available at: <http://link.springer.com/10.1007/s10533-017-0309-x> [Accessed July 9, 2019].
- Klinkhammer G. . and Palmer M. . (1991) Uranium in the oceans: Where it goes and why. *Geochim. Cosmochim. Acta* **55**, 1799–1806. Available at: <https://www.sciencedirect.com/science/article/pii/001670379190024Y> [Accessed November 30, 2018].
- Kononets M., Nilsson M., Tengberg A., Ekeröth N., Hylén A., van de Velde S., Blomqvist S. and Hall P. O. J. (2018) In situ incubations with a benthic chamber lander system: Performance, quality control and capabilities with recommendations for a best practice. *Prog. Oceanogr.* **submitted**.
- Kryc K. A., Murray R. W. and Murray D. W. (2003) Al-to-oxide and Ti-to-organic linkages in biogenic sediment: Relationships to paleo-export production and bulk Al/Ti. *Earth Planet. Sci. Lett.* **211**, 125–141.
- Lee Y. and Tebo B. M. (1994) Cobalt (II) Oxidation by the Marine Manganese (II)-Oxidizing *Bacillus* sp. Strain SG-1. *Appl. Environ. Microbiol.* **60**, 2949–2957.
- Lenstra W. K., Hermans M., Seguret M., Witbaard R., Behrends T., Helmond N. A. G. M. Van, Kraal P., Kuzminov A., Laan P., Severmann S., Teaca A. and Slomp C. P. (2018) The shelf-to-basin iron shuttle in the Black Sea revisited. *Chem. Geol.*, 1–52. Available at: <https://doi.org/10.1016/j.chemgeo.2018.10.024>.
- Liblik T., Naumann M., Alenius P., Hansson M., Lips U., Nausch G., Tuomi L., Wesslander K., Laanemets J. and Viktorsson L. (2018) Propagation of Impact of the Recent Major Baltic Inflows From the Eastern Gotland Basin to the Gulf of Finland. *Front. Mar. Sci.* **5**, 222. Available at: <https://www.frontiersin.org/article/10.3389/fmars.2018.00222/full> [Accessed August 10, 2018].
- Lyons T. W. and Severmann S. (2006) A critical look at iron paleoredox proxies: New insights from modern euxinic marine basins. *Geochim. Cosmochim. Acta* **70**, 5698–5722.
- Mahowald N. M., Hamilton D. S., Mackey K. R. M., Moore J. K., Baker A. R., Scanza R. A. and Zhang Y. (2018) Aerosol trace metal leaching and impacts on marine microorganisms. *Nat. Commun.* **9**, 2614. Available at: <http://www.nature.com/articles/s41467-018-04970-7> [Accessed December 4, 2018].
- Marzocchi U., Bonaglia S., van de Velde S., Hall P. O. J., Risgaard-Petersen N. and Meysman F. J. R. (2018) A Major Baltic Inflow creates a temporal niche for cable bacteria in Eastern Gotland basin sediments. *Environ. Microbiol.* **20**, 3031–3041.
- McLennan S. M. (2001) Relationships between the trace element composition of sedimentary rocks and upper continental crust. *Geochemistry, Geophys. Geosystems* **2**.
- Moffett J. W. and Ho J. (1996) Oxidation of cobalt and manganese in seawater via a common microbially catalyzed pathway. *Geochim. Cosmochim. Acta* **60**, 3415–3424.
- Mohrholz V., Naumann M., Nausch G., Krüger S. and Gräwe U. (2015) Fresh oxygen for the Baltic Sea — An exceptional saline inflow after a decade of stagnation. *J. Mar. Syst.* **148**, 152–166. Available at: <https://www.sciencedirect.com/science/article/pii/S0924796315000457> [Accessed August 10, 2018].
- Morel F. M. M. and Price N. M. (2003) The biogeochemical cycles of trace metals in the oceans. *Science* **300**, 944–7. Available at: <http://www.ncbi.nlm.nih.gov/pubmed/12738853> [Accessed December 12, 2013].
- Morford J. L. and Emerson S. (1999) The geochemistry of redox sensitive trace metals in sediments. *Geochim. Cosmochim. Acta* **63**, 1735–1750. Available at: <https://www.sciencedirect.com/science/article/pii/S001670379900126X> [Accessed February 6, 2019].
- Neretin L. N., Pohl C., Jost G., Leipe T. and Pollehne F. (2003) Manganese cycling in the

- Gotland Deep, Baltic Sea. *Mar. Chem.* **82**, 125–143. Available at: [www.elsevier.com/locate/marchem](http://www.elsevier.com/locate/marchem) [Accessed December 3, 2018].
- Neumann T., Christiansen C., Clasen S., Emeis K.-C. and Kunzendorf H. (1997) Geochemical records of salt-water inflows into the deep basins of the Baltic Sea. *Cont. Shelf Res.* **17**, 95–115. Available at: <https://www.sciencedirect.com/science/article/pii/0278434396000234?via%3Dihub> [Accessed July 20, 2018].
- Neumann T., Heiser U., Leosson M. A. and Kersten M. (2002) Early diagenetic processes during Mn-carbonate formation: evidence from the isotopic composition of authigenic Ca-rhodochrosites of the Baltic Sea. *Geochim. Cosmochim. Acta* **66**, 867–879. Available at: <https://www.sciencedirect.com/science/article/pii/S0016703701008195> [Accessed July 9, 2019].
- Nieuwenhuize J., Maas Y. E. M. and Middelburg J. J. (1994) Rapid analysis of organic carbon and nitrogen in particulate materials. *Mar. Chem.* **45**, 217–224.
- Nilsson M., Kononets M., Ekeröth N., Viktorsson L., Hylén A., Sommer S., Pfannkuche O., Almroth Rosell E., Atamanchuk D., Andersson J., Roos P., Tengberg A. and Hall P. O. J. (2018) Organic carbon recycling in Baltic Sea sediments - An integrated estimate on the system scale based on in situ measurements. *Mar. Chem.* **209**, 81–93.
- Noffke A., Hensen C., Sommer S., Scholz F., Bohlen L., Mosch T., Graco M. and Wallmann K. (2012) Benthic iron and phosphorus fluxes across the Peruvian oxygen minimum zone. *Limnol. Oceanogr.* **57**, 851–867. Available at: <https://aslopubs.onlinelibrary.wiley.com/doi/pdf/10.4319/lo.2012.57.3.0851> [Accessed June 26, 2019].
- O'Connor T. P. and Kester D. R. (1975) Adsorption of copper and cobalt from fresh and marine systems. *Geochim. Cosmochim. Acta* **39**, 1531–1543.
- Pakhomova S. V., Hall P. O. J., Kononets M. Y., Rozanov A. G., Tengberg A. and Vershinin A. V. (2007) Fluxes of iron and manganese across the sediment-water interface under various redox conditions. *Mar. Chem.* **107**, 319–331.
- Piper D. Z. and Perkins R. B. (2004) A modern vs. Permian black shale—the hydrography, primary productivity, and water-column chemistry of deposition. *Chem. Geol.* **206**, 177–197. Available at: <https://www.sciencedirect.com/science/article/pii/S0009254103003905> [Accessed March 12, 2018].
- Point D., Monperrus M., Tessier E., Chauvaud L., Thouzeau G., Jean F., Amice E., Grall J., Leynaert A., Clavier J. and Donard O. F. X. (2007) Biological control of trace metal and organometal benthic fluxes in a eutrophic lagoon (Thau Lagoon, Mediterranean Sea, France). *Estuar. Coast. Shelf Sci.* **72**, 457–471. Available at: <https://www.sciencedirect.com/science/article/pii/S0272771406005324> [Accessed March 23, 2018].
- R Core Team (2017) R: A Language and Environment for Statistical Computing.
- Saito M. A. and Moffett J. W. (2001) Complexation of cobalt by natural organic ligands in the Sargasso Sea as determined by a new high-sensitivity electrochemical cobalt speciation method suitable for open ocean work. *Mar. Chem.* **75**, 49–68.
- Saito M. A. and Moffett J. W. (2002) Temporal and spatial variability of cobalt in the Atlantic Ocean. *Geochim. Cosmochim. Acta* **66**, 1943–1953.
- Scholz F., Baum M., Siebert C., Eroglu S., Dale A. W., Naumann M. and Sommer S. (2018) Sedimentary molybdenum cycling in the aftermath of seawater inflow to the intermittently euxinic Gotland Deep, Central Baltic Sea. *Chem. Geol.* **491**, 27–38. Available at: <https://www.sciencedirect.com/science/article/pii/S0009254118302183> [Accessed June 26, 2019].
- Scholz F., Hensen C., Noffke A., Rohde A., Liebetrau V. and Wallmann K. (2011) Early diagenesis of redox-sensitive trace metals in the Peru upwelling area - response to ENSO-related oxygen fluctuations in the water column. *Geochim. Cosmochim. Acta* **75**, 7257–7276. Available at: <http://dx.doi.org/10.1016/j.gca.2011.08.007>.

- Scholz F., McManus J., Mix A. C., Hensen C. and Schneider R. R. (2014) The impact of ocean deoxygenation on iron release from continental margin sediments. *Nat. Geosci.* **7**, 433–437. Available at: <http://www.nature.com/doi/10.1038/ngeo2162>.
- Scholz F., McManus J. and Sommer S. (2013) The manganese and iron shuttle in a modern euxinic basin and implications for molybdenum cycling at euxinic ocean margins. *Chem. Geol.* **355**, 56–68. Available at: <http://dx.doi.org/10.1016/j.chemgeo.2013.07.006>.
- Severmann S., McManus J., Berelson W. M. and Hammond D. E. (2010) The continental shelf benthic iron flux and its isotope composition. *Geochim. Cosmochim. Acta* **74**, 3984–4004. Available at: <http://dx.doi.org/10.1016/j.gca.2010.04.022>.
- Sheng P. X., Ting Y.-P., Chen J. P. and Hong L. (2004) Sorption of lead, copper, cadmium, zinc, and nickel by marine algal biomass: characterization of biosorptive capacity and investigation of mechanisms. *J. Colloid Interface Sci.* **275**, 131–141. Available at: <https://www.sciencedirect.com/science/article/pii/S0021979704000943> [Accessed July 1, 2019].
- Sommer S., Clemens D., Yücel M., Pfannkuche O., Hall P. O. J., Almroth-Rosell E., Schulz-Vogt H. N. and Dale A. W. (2017) Major Bottom Water Ventilation Events Do Not Significantly Reduce Basin-Wide Benthic N and P Release in the Eastern Gotland Basin (Baltic Sea). *Front. Mar. Sci.*
- Sternbeck J. and Sohlenius G. (1997) Authigenic sulfide and carbonate mineral formation in Holocene sediments of the Baltic Sea. *Chem. Geol.* **135**, 55–73. Available at: <https://www.sciencedirect.com/science/article/pii/S0009254196001040> [Accessed July 9, 2019].
- Suess E. (1979) Mineral phases formed in anoxic sediments by microbial decomposition of organic matter. *Geochim. Cosmochim. Acta* **43**, 339–352. Available at: <https://www.sciencedirect.com/science/article/pii/0016703779901996?via%3Dihub> [Accessed July 20, 2018].
- Sulu-gambari F., Roepert A., Jilbert T., Hagens M., Meysman F. J. R. and Slomp C. P. (2017) Molybdenum dynamics in sediments of a seasonally hypoxic coastal marine basin. *Chem. Geol.* **466**, 627–640.
- Sundby B., Anderson L. G., Hall P. O. J., Iverfeldt A., Rutgers Van Der Loeff M. M. and Westerlund S. F. G. (1986) The effect of oxygen on release and uptake of cobalt, manganese, iron and phosphate at the sediment-water interface. *Geochim. Cosmochim. Acta* **50**, 1281–1288.
- Suraj G., Iyer C. S. P. and Lalithambika M. (1998) Adsorption of cadmium and copper by modified kaolinites. *Appl. Clay Sci.* **13**, 293–306. Available at: <https://www.sciencedirect.com/science/article/pii/S016913179800043X> [Accessed July 3, 2019].
- Tengberg A., Stahl H., Gust G., Müller V., Arning U., Andersson H. and Hall P. O. J. (2004) Intercalibration of benthic flux chambers I. Accuracy of flux measurements and influence of chamber hydrodynamics. *Prog. Oceanogr.* **60**, 1–28. Available at: <https://www.sciencedirect.com/science/article/pii/S0079661104000023?via%3Dihub> [Accessed August 10, 2018].
- Thamdrup B. (2000) Bacterial Manganese and Iron Reduction in Aquatic Sediments. In *Advances in Microbial Ecology* (ed. B. Schink). Luwer Academic/Plenum Publishers, New York. pp. 41–84.
- Thamdrup B., Fossing H. and Jorgensen B. B. (1994a) Manganese, iron, and sulfur cycling in a coastal marine sediment, Aarhus Bay, Denmark. *Geochim. Cosmochim. Acta* **58**, 5115–5129.
- Thamdrup B., Glud R. N. and Hansen J. W. (1994b) Manganese oxidation and in situ manganese fluxes from a coastal sediment. *Geochim. Cosmochim. Acta* **58**, 2563–2570.
- Thibault de Chanvalon A., Metzger E., Mouret A., Knoery J., Geslin E. and Meysman F. J. R. (2017) Two dimensional mapping of iron release in marine sediments at submillimetre scale. *Mar. Chem.* **191**, 34–49. Available at: <http://dx.doi.org/10.1016/j.marchem.2016.04.003>.



- Tribovillard N., Algeo T. J., Lyons T. and Riboulleau A. (2006) Trace metals as paleoredox and paleoproductivity proxies: An update. *Chem. Geol.* **232**, 12–32.
- Tribovillard N., Riboulleau A., Lyons T. and Baudin F. (2004) Enhanced trapping of molybdenum by sulfurized marine organic matter of marine origin in Mesozoic limestones and shales. *Chem. Geol.* **213**, 385–401.
- Turetta C., Capodaglio G., Cairns W., Rabar S. and Cescon P. (2005) Benthic fluxes of trace metals in the lagoon of Venice. *Microchem. J.* **79**, 149–158. Available at: <https://www.sciencedirect.com/science/article/pii/S0026265X04001250> [Accessed March 23, 2018].
- van de Velde S. and Meysman F. J. R. (2016) The influence of bioturbation on iron and sulphur cycling in marine sediments: a model analysis. *Aquat. Geochemistry* **22**, 469–504.
- Vijayaraghavan K., Jegan J., Palanivelu K. and Velan M. (2005) Biosorption of copper, cobalt and nickel by marine green alga *Ulva reticulata* in a packed column. *Chemosphere* **60**, 419–426. Available at: <https://www.sciencedirect.com/science/article/pii/S0045653505000238> [Accessed July 1, 2019].
- Vorliceck T. P., Kahn M. D., Kasuya Y. and Helz G. R. (2004) Capture of molybdenum in pyrite-forming sediments: Role of ligand-induced reduction by polysulfides. *Geochim. Cosmochim. Acta* **68**, 547–556.
- Waite T. D., Davis J. A., Payne T. E., Waychunas G. A. and Xu N. (1994) Uranium(VI) adsorption to ferrihydrite: Application of a surface complexation model. *Geochim. Cosmochim. Acta* **58**, 5465–5478. Available at: <https://www.sciencedirect.com/science/article/pii/0016703794902437> [Accessed June 19, 2019].
- Wallmann K. (1992) Solubility of cadmium and cobalt in a post-oxic or sub-oxic sediment suspension. *Hydrobiologia* **235/236**, 611–622.
- Wang Z., Lee S.-W., Catalano J. G., Lezama-Pacheco J. S., Bargar J. R., Tebo B. M. and Giammar D. E. (2013) Adsorption of Uranium(VI) to Manganese Oxides: X-ray Absorption Spectroscopy and Surface Complexation Modeling. *Environ. Sci. Technol.* **47**, 850–858. Available at: <http://pubs.acs.org/doi/10.1021/es304454g> [Accessed June 19, 2019].
- Wanty R. B. and Goldhaber M. B. (1992) Thermodynamics and kinetics of reactions involving vanadium in natural systems: Accumulation of vanadium in sedimentary rocks. *Geochim. Cosmochim. Acta* **56**, 1471–1483. Available at: <https://www.sciencedirect.com/science/article/pii/0016703792902177> [Accessed March 12, 2018].
- Wehrli B. and Stumm W. (1989a) Vanadyl in natural waters: Adsorption and hydrolysis promote oxygenation. *Geochim. Cosmochim. Acta* **53**, 69–77.
- Wehrli B. and Stumm W. (1989b) Vanadyl in natural waters: Adsorption and hydrolysis promote oxygenation. *Geochim. Cosmochim. Acta* **53**, 69–77. Available at: <https://www.sciencedirect.com/science/article/pii/0016703789902731> [Accessed March 13, 2018].
- Westerlund S. F. G., Anderson L. G., Hall P. O. J., Iverfeldt A., Rutgers Van Der Loeff M. M. and Sundby B. (1986) Benthic fluxes of cadmium, copper, nickel, zinc and lead in the coastal environment. *Geochim. Cosmochim. Acta* **50**, 1289–1296.
- Zheng Y., Anderson R. F., van Geen A. and Fleisher M. Q. (2002) Remobilization of authigenic uranium in marine sediments by bioturbation. *Geochim. Cosmochim. Acta* **66**, 1759–1772. Available at: <https://www.sciencedirect.com/science/article/pii/S0016703701008869> [Accessed December 4, 2018].